

There are No Bit Parts for Sign Bits in Black-Box Attacks

Abdullah Al-Dujaili
Una-May O'Reilly
CSAIL, MIT, USA

ALDUJAIL@MIT.EDU
UNAMAY@CSAIL.MIT.EDU

Abstract

Machine learning models are vulnerable to adversarial examples. In this paper, we are concerned with black-box adversarial attacks, where only loss-oracle access to a model is available and a high model evasion rate is the attacker's ultimate objective. At the heart of black-box adversarial attack is the gradient estimation problem with standard query complexity $O(n)$, where n is the number of data features. Recent work has developed query-efficient gradient estimation schemes by exploiting data- and/or time-dependent priors. Practically, sign-based optimization has shown to be effective in both training deep nets as well as attacking them in a white-box setting. Therefore, instead of a gradient estimation view of black-box adversarial attacks, we view the black-box adversarial attack problem as estimating the gradient's sign bits. This shifts the view from continuous to binary black-box optimization and theoretically guarantees a lower query complexity of $\Omega(n/\log_2(n+1))$ when given access to a Hamming loss oracle. We present three algorithms to estimate the gradient sign bits given a limited number of queries to the loss oracle. They are based on three properties of the directional derivative of the loss in the direction of $\{\pm 1\}^n$ vectors. Using one of our proposed algorithms to craft black-box adversarial examples, we demonstrate evasion rate experiments on standard models trained on the MNIST, CIFAR10, and IMAGENET datasets that set new state-of-the-art results for query-efficient black-box attacks in the ℓ_∞ and ℓ_2 metrics. Averaged overall the datasets and metrics, our attack fails $3.8\times$ less often, and spends in total $2.5\times$ fewer queries than the current state-of-the-art attacks combined given a budget of 10,000 queries per attack attempt.¹ On a public MNIST black-box attack challenge, our attack achieves the highest evasion rate surpassing all of the submitted attacks.² Notably, our attack is hyperparameter-free (no hyperparameter tuning) and does not employ any data-/time-dependent prior, the latter fact suggesting that the number of queries can further be reduced.

Keywords: Deep Nets, Adversarial Examples, Black-Box Optimization, Zeroth-Order Optimization

1. Introduction

1.1 Problem

Deep Neural Networks (DNNs) are vulnerable to adversarial examples, which are malicious inputs designed to fool the network's prediction—see (Biggio and Roli, 2018) for a comprehensive, recent overview of adversarial examples. Research on generating these malicious inputs started in the *white-box* setting, where access to the gradients of the models was assumed. Since the gradient points to the direction of steepest ascent, a malicious input

¹The code for reproducing our work will be made available at <https://github.com/ALFA-group>.

²https://github.com/MadryLab/mnist_challenge

can be perturbed along that gradient to maximize the network’s loss, thereby fooling its prediction. The assumption of access to the underlying gradient does not however reflect real world scenarios. Attacks to a realistic, more restrictive *black-box* threat model, which does not assume access to gradients, have since been studied as summarized in Section 1.2.

Central to the approach of generating adversarial examples in a *black-box* threat model is estimating the gradients of the model being attacked. In estimating these gradients (their magnitudes and signs), the community at large has focused on formulating it as a problem in continuous optimization. Their works seek to reduce the query complexity from the standard $O(n)$, where n is the number of input features/covariates. In this paper, we take a different view and focus on estimating just the sign of the gradient by reformulating the problem as minimizing the Hamming distance to the gradient sign. Given access to a Hamming distance oracle, this view guarantees a query complexity of $\Omega(n/\log_2(n+1))$: an order of magnitude lesser than the full gradient estimation’s query complexity for most practically-occurring input dimensions n . Our key objective is to answer the following:

Is it possible to estimate only the sign of the gradient with such query efficiency and generate adversarial examples as effective as those generated by full gradient estimation approaches?

We propose a novel formulation which attempts to achieve this by exploiting some properties of the directional derivative of the loss function of the model under attack, and through rigorous empirical evaluation we show our approach outperforms state of the art full gradient estimation techniques. We also identify several key areas of research which we believe will help the community towards query-efficient adversarial attacks and gradient-free optimization.

1.2 Related Work

We organize the related work in two themes, namely *Adversarial Example Generation* and *Sign-Based Optimization*.

Adversarial Example Generation. This literature can be organized as generating examples in either a *white-box* or a *black-box* setting. Nelson et al. (2012) provide a theoretical framework to analyze adversarial querying in a *white-box* setting. Following the works of Biggio et al. (2013) and Goodfellow et al. (2015) who introduced the fast gradient sign method (FGSM), several methods to produce adversarial examples have been proposed for various learning tasks and threat perturbation constraints (Al-Dujaili et al., 2018; Carlini and Wagner, 2017; Hayes and Danezis, 2017; Huang et al., 2018; Kurakin et al., 2017; Moosavi-Dezfooli et al., 2016; Shamir et al., 2019). These methods assume a *white-box* setup and are not the focus of this work. An approach, which has received the community’s attention, involves learning adversarial examples for one model (with access to its gradient information) to transfer them against another (Liu et al., 2016; Papernot et al., 2017). As an alternative to the transferability phenomenon, Xiao et al. (2018) use a Generative Adversarial Network (GAN) to generate adversarial examples which are based on small norm-bounded perturbations. Both approaches involve learning on a different model, which is expensive, and does not lend itself to comparison in our setup, where we directly query the model of interest. Among works which generate examples in a *black-box* setting through iterative

optimization schemes, [Narodytska and Kasiviswanathan \(2017\)](#) showed how a naïve policy of perturbing random segments of an image achieved adversarial example generation. They do not use any gradient information. [Bhagoji et al. \(2017\)](#) reduce the dimensions of the feature space using Principal Component Analysis (PCA) and random feature grouping, before estimating gradients. This enables them to bound the number of queries made. [Chen et al. \(2017\)](#) introduced a principled approach to solving this problem using gradient based optimization. They employ finite differences, a zeroth-order optimization tool, to estimate the gradient and then use it to design a gradient-based attack on models. While this approach successfully generates adversarial examples, it is expensive in the number of queries made to the model. [Ilyas et al. \(2018\)](#) substitute traditional finite differences methods with Natural Evolutionary Strategies (NES) to obtain an estimate of the gradient. [Tu et al. \(2018\)](#) provide an adaptive random gradient estimation algorithm that balances query counts and distortion, and introduces a trained auto-encoder to achieve attack acceleration. [Ilyas et al. \(2019\)](#) extend this line of work by proposing the idea of gradient priors. Our work contrasts the general approach used by these works. We investigate whether just estimating the *sign* of the gradient suffices to efficiently generate examples.

Sign-Based Optimization. In the context of general-purpose continuous optimization methods, sign-based stochastic gradient descent was studied in both zeroth- and first-order setups. In the latter, [Bernstein et al. \(2018\)](#) analyzed `signSGD`, a sign-based Stochastic Gradient Descent, and showed that it enjoys a faster empirical convergence than `SGD` in addition to the cost reduction of communicating gradients across multiple workers. [Liu et al. \(2019\)](#) extended `signSGD` to zeroth-order setup with the `ZO-SignSGD` algorithm. `ZO-SignSGD` requires \sqrt{n} times more iterations than `signSGD`, leading to a convergence rate of $O(\sqrt{n/T})$, where n is the number of optimization variables, and T is the number of iterations.

Adversarial Examples Meet Sign-based Optimization. In the context of adversarial examples generation, the effectiveness of sign of the gradient coordinates was noted in both white- and black-box settings. In the former, the Fast Gradient Sign Method (FGSM)—which is algorithmically similar to `signSGD`—was proposed to generate white-box adversarial examples ([Goodfellow et al., 2015](#)). [Ilyas et al. \(2019\)](#) examined a noisy version of FGSM to address the question of *How accurate of a gradient estimate is necessary to execute a successful attack on a neural net*. In Figure 1, we reproduce their experiment on an **IMAGENET**-based model—Plot (c)—and extended it to the **MNIST** and **CIFAR10** datasets—Plots (a) and (b). Observe that estimating the sign of the top 30% gradient coordinates (in terms of their magnitudes) is enough to achieve a misclassification rate of $\sim 70\%$. Furthermore, `ZO-SignSGD` ([Liu et al., 2019](#)) was shown to perform better than NES at generating adversarial examples against a black-box neural network on the **MNIST** dataset.

1.3 Our Contributions

Motivated by i) the practical effectiveness of the gradient sign information; and that ii) the gradient sign can be recovered with a lower query complexity than to retrieve both its sign and magnitude (as we will show herein), we view the black-box adversarial attack problem as estimating the gradient’s sign bits. This shift from continuous to binary black-box optimization leads to the following contributions at the intersection of adversarial machine learning and black-box (zeroth-order) optimization:

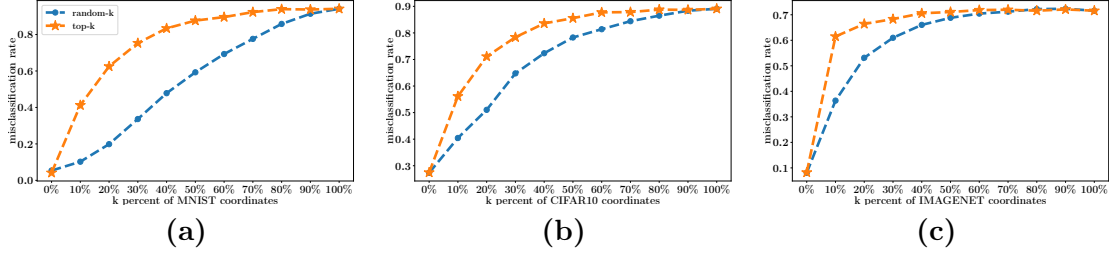


Figure 1: Misclassification rate of three neural nets (for (a) **MNIST**, (b) **CIFAR10**, and (c) **IMAGENET**, respectively) on the *noisy FGSM*’s adversarial examples as a function of correctly estimated coordinates of $\text{sign}(\nabla_{\mathbf{x}} f(\mathbf{x}, y))$ on random 1000 images from the corresponding evaluation dataset. Across all the models, estimating the sign of the top 30% gradient coordinates (in terms of their magnitudes) is enough to achieve a misclassification rate of $\sim 70\%$. More details can be found in Appendix A.

- We present three properties of the directional derivative of the loss function of the model under attack in the direction of $\{\pm 1\}^n$ vectors, and propose methods to estimate the gradient sign bits exploiting these properties. Namely,
 1. Property 1 shows that the directional derivative in the direction of a sign vector $\mathbf{q} \in \{-1, +1\}^n$ is an affine transformation of the Hamming distance between \mathbf{q} and the gradient sign vector. This suggests that if we can recover the Hamming distance from the directional derivative, then the gradient sign bits can be recovered with a query complexity of $\Omega(n/\log_2(n+1))$ using any off-the-shelf efficient Hamming search strategy.
 2. Property 2 shows that the directional derivative is locally smooth around the gradient sign. This lets us employ the *optimism in the face of uncertainty* principle in estimating the gradient sign. Through the use of hierarchical bandits, we show that the knowledge of this smoothness is not required and provide a finite-time upper bound on the quality of the estimation at the expense of searching over the 2^n possible sign vectors.
 3. Property 3 shows that the directional derivative is separable with respect to coordinates of a sign vector \mathbf{q} . Based on this property, we devise a divide-and-conquer algorithm, which we refer to as **SignHunter**, that reduces the search complexity from 2^n to $O(n)$. When given a budget of $O(2n)$ queries, **SignHunter** is guaranteed to perform at least as well as **FGSM** (Goodfellow et al., 2015), which has access to the model’s gradient.
- Through rigorous empirical evaluation, Property 3 (and hence **SignHunter**) is found to be the most effective in crafting black-box adversarial examples. In particular,
 1. To exploit Property 1, we propose an estimation of the Hamming distance (to the gradient sign) oracle from the finite difference of model’s loss value queries, and provide an empirical motivation and evaluation of the same. We find that efficient Hamming search strategies from the literature (e.g., Maurer (2009)) are

not robust to approximation error of the proposed Hamming distance estimation, and hence no guarantees can be made about the estimated sign vector.

2. Despite being theoretically-founded, the approach exploiting Property 2 is slow and not scalable for most practically-occurring input dimensions n .
 3. Through experiments on **MNIST**, **CIFAR10**, and **IMAGENET** for both ℓ_∞ and ℓ_2 threat constraints, **SignHunter** yields black-box attacks that are $2.5\times$ more query efficient and $3.8\times$ less failure-prone than the state of the art attacks combined. On a public black-box attack challenge, our approach achieves the highest evasion rate surpassing techniques based on transferability, ensembling, and generative adversarial networks.
- Finally, we release a software framework³ to systematically benchmark adversarial black-box attacks on DNNs for **MNIST**, **CIFAR10**, and **IMAGENET** datasets in terms of their success rate, query count, and other related metrics. This was motivated by the problem we faced in comparing approaches from the literature, where different researchers evaluated their approaches on different datasets, metrics, and setups—e.g., some compared only on **MNIST** while others considered **CIFAR10** and **IMAGENET**.

The rest of the paper is structured as follows. First, a formal background is presented in Section 2. Section 3 describes our approach for black-box adversarial attacks by examining three properties of the loss’s directional derivative of the model under attack. Experiments are discussed in Section 4. We evaluate the effectiveness of the approach against one of the defenses developed against adversarial examples in Section 5. Finally, conclusions are drawn and future work is outlined in Section 6.

2. Formal Background

2.1 Notation.

Let n denote the dimension of a neural network’s input. Denote a hidden n -dimensional binary code by \mathbf{q}^* . That is, $\mathbf{q}^* \in \mathcal{H} \equiv \{-1, +1\}^n$. The response of the Hamming (distance) oracle \mathcal{O} to the i th query $\mathbf{q}^{(i)} \in \mathcal{H}$ is denoted by $r^{(i)} \in \{0, \dots, n\}$ and equals the Hamming distance

$$r^{(i)} = \|\mathbf{q}^{(i)} - \mathbf{q}^*\|_H, \quad (1)$$

where the Hamming norm $\|\mathbf{v}\|_H$ is defined as the number of non-zero entries of vector \mathbf{v} . We also refer to \mathcal{O} as the *noiseless* Hamming oracle, in contrast to the *noisy* Hamming oracle $\tilde{\mathcal{O}}$, which returns noisy versions of \mathcal{O} ’s responses as we will see shortly. I_n is the $n \times n$ identity matrix. The query ratio $\rho \in (0, 1]$ is defined as m/n where m is the number of queries to \mathcal{O} required to retrieve \mathbf{q}^* . Furthermore, denote the directional derivative of some function f at a point \mathbf{x} in the direction of a vector \mathbf{v} by $D_{\mathbf{v}}f(\mathbf{x}) \equiv \mathbf{v}^T \nabla_{\mathbf{x}} f(\mathbf{x})$ which often can be approximated by the *finite difference* method. That is, for $\delta > 0$, we have

$$D_{\mathbf{v}}f(\mathbf{x}) = \mathbf{v}^T \nabla_{\mathbf{x}} f(\mathbf{x}) \approx \frac{f(\mathbf{x} + \delta \mathbf{v}) - f(\mathbf{x})}{\delta}. \quad (2)$$

³This builds on other open-source frameworks such as the MNIST and CIFAR challenges (Madry et al., 2017).

Let $\Pi_S(\cdot)$ be the projection operator onto the set S , $B_p(\mathbf{x}, \epsilon)$ be the ℓ_p ball of radius ϵ around \mathbf{x} . Next, we provide lower and upper bounds on the query ratio ρ .

2.2 Bounds on the Query Ratio ρ

Lower Bound on ρ . Using a packing argument, [Vaishampayan \(2012\)](#) proved the following lower bound on query ratio ρ .

Theorem 1 ([Vaishampayan, 2012, Theorem 1](#)) *For the noiseless Hamming oracle \mathcal{O} , the query ratio must satisfy*

$$\rho = m/n \geq \frac{1}{\log_2(n+1)}$$

for any sequence of m queries that determine every n -dimensional binary code \mathbf{q}^ uniquely.*

Proof See ([Vaishampayan, 2012, Page 4](#)). ■

Exact Solution with $\rho = 1$. In the following theorem, we show that no more than n queries are required to retrieve the hidden n -dimensional binary code \mathbf{q}^* .

Theorem 2 *A hidden n -dimensional binary code $\mathbf{q}^* \in \mathcal{H}$ can be retrieved exactly with no more than n queries to the noiseless Hamming oracle \mathcal{O} .*

Proof The key element of this proof is that the Hamming distance between two n -dimensional binary codes $\mathbf{q}, \mathbf{q}^* \in \mathcal{H}$ can be written as

$$r = \|\mathbf{q} - \mathbf{q}^*\|_H = \frac{1}{2}(n - \mathbf{q}^T \mathbf{q}^*). \quad (3)$$

Let Q be an $n \times n$ matrix where the i th row is the i th query code $\mathbf{q}^{(i)}$. Likewise, let $r^{(i)}$ be the corresponding i th query response, and \mathbf{r} is the concatenating vector. In matrix form, we have

$$\mathbf{q}^* = Q^{-1}(nI_n - 2\mathbf{r}),$$

where Q is invertible if we construct linearly independent queries $\{\mathbf{q}^{(i)}\}_{1 \leq i \leq n}$. ■

In Figure 2, we plot the bounds above for $n = \{1, \dots, 10\}$, along with two search strategies for \mathbf{q}^* using the Hamming oracle: i) **Maurer's** [Maurer \(2009\)](#); and ii) search by **Elimination** which, after response $r^{(i)}$ to query $\mathbf{q}^{(i)}$, eliminates all binary codes $\mathbf{q} \in \mathcal{H}$ with $\|\mathbf{q} - \mathbf{q}^{(i)}\|_H \neq r^{(i)}$ in an iterative manner. Note that **Elimination** is a naive technique that is not scalable with n .

2.3 Gradient Estimation Problem: a Hamming Distance View

At the heart of black-box adversarial attacks is generating a *perturbation vector* to slightly modify the original input \mathbf{x} so as to fool the network prediction of its true label y . Put it differently, an adversarial example \mathbf{x}' maximizes the network's loss $L(\mathbf{x}', y)$ but still remains ϵ_p -close to the original input \mathbf{x} . Although the loss function L can be non-concave, gradient-based techniques are often very successful in crafting an adversarial example ([Madry](#)

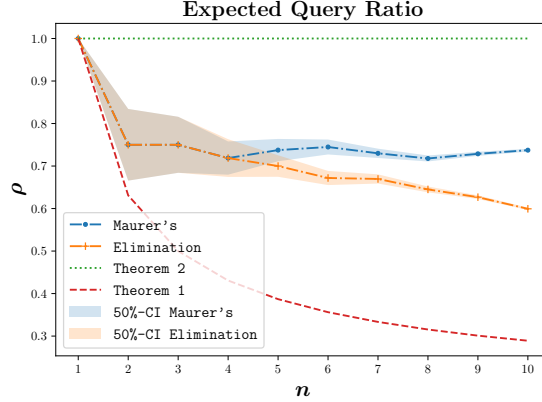


Figure 2: Expected Query Ratios for $n = \{1, \dots, 10\}$ with the *noiseless* Hamming oracle \mathcal{O} .

et al., 2017). That is, to set the perturbation vector as a step in the direction of $\nabla_{\mathbf{x}}L(\mathbf{x}, y)$. Subsequently, the bulk of black-box attack methods sought to *estimate the gradient* by querying an oracle that returns, for a given input/label pair (\mathbf{x}, y) , the value of the network’s loss $L(\mathbf{x}, y)$. Using only such value queries, the basic approach relies on the *finite difference method* to approximate the directional derivative (Eq. 2) of the function L at the input/label pair (\mathbf{x}, y) in the direction of a vector \mathbf{v} , which corresponds to $\mathbf{v}^T \nabla_{\mathbf{x}}L(\mathbf{x}, y)$. With n linearly independent vectors $\{\mathbf{v}^{(i)T} \nabla_{\mathbf{x}}L(\mathbf{x}, y) = d^{(i)}\}_{1 \leq i \leq n}$, one can construct a linear system of equations to recover the full gradient. Clearly, this approach’s query complexity is $\Omega(n)$, which can be prohibitively expensive for large n (e.g., $n = 268,203$ for the **IMAGENET** dataset). Moreover, the queries are not adaptive, where one may make use of the past queries’ responses to construct the new query and recover the full gradient with less queries. Recent works tried to mitigate this issue by exploiting data- and/or time-dependent priors (Ilyas et al., 2018, 2019; Tu et al., 2018).

The lower bound of Theorem 1 on the query complexity of a Hamming oracle \mathcal{O} to find a hidden vector \mathbf{q}^* suggests the following: *instead of estimating the full gradient (sign and magnitude) and apart from exploiting any data- or time-dependent priors; why do we not focus on estimating its sign?* After all, simply leveraging (noisy) sign information of the gradient yields successful attacks; see Figure 1. Therefore, our interest in this paper is the *gradient sign estimation problem*, which we formally define next, breaking away from the general trend of the *continuous optimization view* in constructing black-box adversarial attacks, manifested by the focus on the *full gradient estimation problem*.

Definition 1 (*Gradient Sign Estimation Problem*) For an input/label pair (\mathbf{x}, y) and a loss function L , let $\mathbf{g}^* = \nabla_{\mathbf{x}}L(\mathbf{x}, y)$ be the gradient of L at (\mathbf{x}, y) and $\mathbf{q}^* = \text{sign}(\mathbf{g}^*) \in \mathcal{H}$ be the sign bit vector of \mathbf{g}^* .⁴ Then the goal of the gradient sign estimation problem is to find a

⁴Without loss of generality, we encode the sign bit vector in $\mathcal{H} \equiv \{-1, +1\}^n$ rather than $\{0, 1\}^n$. This is a common representation in sign-related literature. Note that the standard sign function has the range of $\{-1, 0, +1\}$. Here, we use the non-standard definition (Zhao, 2018) whose range is $\{-1, +1\}$. This follows from the observation that DNNs’ gradients are not sparse (Ilyas et al., 2019, Appendix B.1).

binary⁵ vector $\mathbf{q} \in \mathcal{H}$ minimizing the Hamming norm

$$\min_{\mathbf{q} \in \mathcal{H}} \|\mathbf{q} - \mathbf{q}^*\|_H, \quad (4)$$

or equivalently maximizing the directional derivative

$$\max_{\mathbf{q} \in \mathcal{H}} D_{\mathbf{q}} L(\mathbf{x}, y), \quad (5)$$

from a limited number of (possibly adaptive) function value queries $L(\mathbf{x}', y)$.

In the next section, we set to tackle the problem above leveraging three properties of the loss directional derivative $D_{\mathbf{q}} L(\mathbf{x}, y)$ which, in the black-box setup, is approximated by finite difference of loss value queries $L(\mathbf{x}', y)$.

Remark 1 Recall that our definition of the Hamming distance here is over the binary vectors (Eq. 1), a formal statement of the gradient sign estimation problem. In contrast, Shamir et al. (2019) consider the Hamming distance in defining the ℓ_0 threat perturbation constraint: if the threat perturbation constraint is k , only k data features (pixels) are allowed to be changed, and each one of them can change a lot.

3. A Framework for Estimating Sign of the Gradient from Loss Oracles

Our interest in this section is to estimate the gradient sign bits of the loss function L of the model under attack at an input/label pair (\mathbf{x}, y) from a limited number of loss value queries $L(\mathbf{x}', y)$. To this end, we examine the basic concept of directional derivatives that has been employed in recent black-box adversarial attacks. Particularly, we present three approaches to estimate the gradient sign bits based on three properties of the directional derivative $D_{\mathbf{q}} L(\mathbf{x}, y)$ of the loss in the direction of a sign vector $\mathbf{q} \in \mathcal{H}$.

3.1 Approach 1: Loss Oracle as a Noisy Hamming Oracle

The directional derivative of the loss function L at (\mathbf{x}, y) in the direction of a binary code \mathbf{q} can be written as

$$\begin{aligned} D_{\mathbf{q}} L(\mathbf{x}, y) &= \mathbf{q}^T \mathbf{g}^* \\ &= \sum_{i \in \mathcal{I}_{\mathbf{q}}^+} |g_i^*| - \sum_{i \in \mathcal{I}_{\mathbf{q}}^-} |g_i^*| \\ &= |\mathcal{I}_{\mathbf{q}}^+| \bar{g}_{\mathcal{I}_{\mathbf{q}}^+} - |\mathcal{I}_{\mathbf{q}}^-| \bar{g}_{\mathcal{I}_{\mathbf{q}}^-}, \end{aligned} \quad (6)$$

where $\mathcal{I}_{\mathbf{q}}^+ \equiv \{i \mid i \in [n], q_i^* = q_i\}$, $\mathcal{I}_{\mathbf{q}}^- \equiv [n] \setminus \mathcal{I}_{\mathbf{q}}^+$. Note that $|\mathcal{I}_{\mathbf{q}}^+| + |\mathcal{I}_{\mathbf{q}}^-| = n$. The quantities $\bar{g}_{\mathcal{I}_{\mathbf{q}}^+}$ and $\bar{g}_{\mathcal{I}_{\mathbf{q}}^-}$ are the means of $\{|g_i|\}_{i \in \mathcal{I}_{\mathbf{q}}^+}$ and $\{|g_i|\}_{i \in \mathcal{I}_{\mathbf{q}}^-}$, respectively. Observe that $|\mathcal{I}_{\mathbf{q}}^-| = \|\mathbf{q} - \mathbf{q}^*\|_H$: the Hamming distance between \mathbf{q} and the gradient sign \mathbf{q}^* . In other words, the directional derivative $D_{\mathbf{q}} L(\mathbf{x}, y)$ has the following property.

⁵Throughout the paper, we use the terms binary vectors and sign vectors/bits interchangeably.

Property 1 *The directional derivative $D_{\mathbf{q}}L(\mathbf{x}, y)$ of the loss function L at an input/label pair (\mathbf{x}, y) in the direction of a binary code \mathbf{q} can be written as an affine transformation of the Hamming distance between \mathbf{q} and \mathbf{q}^* . Formally, we have*

$$D_{\mathbf{q}}L(\mathbf{x}, y) = n\bar{g}_{\mathcal{I}_{\mathbf{q}}^+} - (\bar{g}_{\mathcal{I}_{\mathbf{q}}^-} + \bar{g}_{\mathcal{I}_{\mathbf{q}}^+})\|\mathbf{q} - \mathbf{q}^*\|_H \quad (7)$$

If we can recover the Hamming distance from the directional derivative based on Eq. 7, efficient Hamming search strategies—e.g., (Maurer, 2009)—can then be used to recover the gradient sign bits \mathbf{q}^* with a query complexity $\Omega(n/\log_2(n+1))$ as stated in Theorem 1. However, not all terms of Eq. 7 is known to us. While n is the number of data features (known a priori) and $D_{\mathbf{q}}L(\mathbf{x}, y)$ is available through a finite difference oracle, $\bar{g}_{\mathcal{I}_{\mathbf{q}}^+}$ and $\bar{g}_{\mathcal{I}_{\mathbf{q}}^-}$ are not known. Here, we propose to approximate these values by their Monte Carlo estimates: averages of the magnitude of sampled gradient components. Our assumption is that the magnitudes of gradient coordinates are not very different from each other, and hence a Monte Carlo estimate is good enough (with small variance). Our experiments on **MNIST**, **CIFAR10**, and **IMAGENET** confirm the same—see Figure 13 in the supplement.

To use the i th gradient component g_i^* as a sample for our estimation, one can construct two binary codes \mathbf{u} and \mathbf{v} such that *only* their i th bit is different, i.e., $\|\mathbf{u} - \mathbf{v}\|_H = 1$. Thus, we have

$$|g_i^*| = \frac{|D_{\mathbf{u}}L(\mathbf{x}, y) - D_{\mathbf{v}}L(\mathbf{x}, y)|}{2} \quad (8)$$

$$q_i^* = \text{sign}(g_i^*) = \begin{cases} u_i & \text{if } D_{\mathbf{u}}L(\mathbf{x}, y) > D_{\mathbf{v}}L(\mathbf{x}, y), \\ v_i & \text{otherwise.} \end{cases} \quad (9)$$

Let \mathcal{D} be the set of indices of gradient components we have recovered—magnitude and sign—so far through Eq. 8 and Eq. 9. Then,

$$\bar{g}_{\mathcal{I}_{\mathbf{q}}^+} \approx \frac{1}{|\mathcal{D}_{\mathbf{q}}^+|} \sum_{d \in \mathcal{D}_{\mathbf{q}}^+} |g_d^*|, \quad (10)$$

$$\bar{g}_{\mathcal{I}_{\mathbf{q}}^-} \approx \frac{1}{|\mathcal{D}_{\mathbf{q}}^-|} \sum_{d \in \mathcal{D}_{\mathbf{q}}^-} |g_d^*|, \quad (11)$$

where $\mathcal{D}_{\mathbf{q}}^+ \equiv \{d \mid d \in \mathcal{D}, q_d^* = q_i\}$ and $\mathcal{D}_{\mathbf{q}}^- \equiv \mathcal{D} \setminus \mathcal{D}_{\mathbf{q}}^+$.⁶ As a result, the Hamming distance between \mathbf{q} and the gradient sign \mathbf{q}^* can be approximated with the following quantity, which we refer to as the *noisy* Hamming oracle $\hat{\mathcal{O}}$.

$$\|\mathbf{q} - \mathbf{q}^*\|_H \approx \frac{\frac{n}{|\mathcal{D}_{\mathbf{q}}^+|} \sum_{d \in \mathcal{D}_{\mathbf{q}}^+} |g_d^*| - D_{\mathbf{q}}L(\mathbf{x}, y)}{\frac{1}{|\mathcal{D}_{\mathbf{q}}^+|} \sum_{d \in \mathcal{D}_{\mathbf{q}}^+} |g_d^*| + \frac{1}{|\mathcal{D}_{\mathbf{q}}^-|} \sum_{d \in \mathcal{D}_{\mathbf{q}}^-} |g_d^*|} \quad (12)$$

We empirically evaluated the quality of $\hat{\mathcal{O}}$'s responses on a toy problem where we controlled the magnitude spread/concentration of the gradient coordinates with m being the number of

⁶It is possible that one of $\mathcal{D}_{\mathbf{q}}^+$ and $\mathcal{D}_{\mathbf{q}}^-$ will \emptyset (e.g., when we only have one sample). In this case, we make the approximation as $\bar{g}_{\mathcal{I}_{\mathbf{q}}^+} = \bar{g}_{\mathcal{I}_{\mathbf{q}}^-} \approx \frac{1}{|\mathcal{D}|} \sum_{d \in \mathcal{D}} |g_d^*|$.

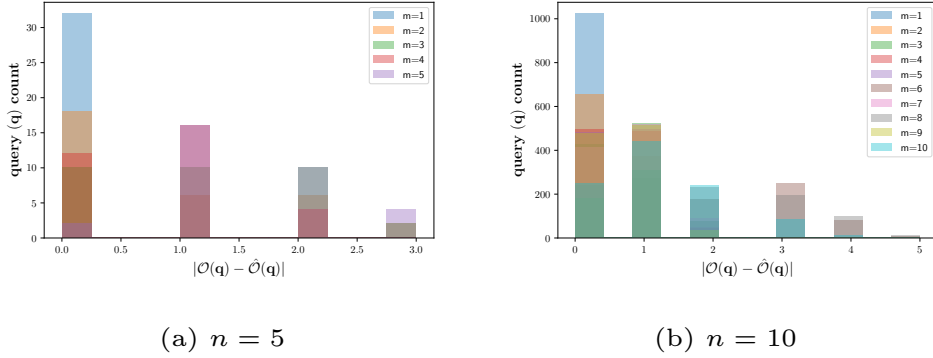


Figure 3: The error distribution of the *noisy* Hamming oracle $\hat{\mathcal{O}}$ (right side of Eq. 12) compared to the *noiseless* counterpart \mathcal{O} (left side of Eq. 12) as a function of the number of unique values (magnitudes) of the gradient coordinates m . Here, $L(\mathbf{x}, y)$ has the form $\mathbf{c}^T \mathbf{x}$. That is, $m = |\text{uniq}(|\mathbf{c}|)| \leq n$ with $n \in \{5, 10\}$ being the input length. With $m = 1$, the estimation is exact ($\hat{\mathcal{O}} = \mathcal{O}$) for all the binary code queries \mathbf{q} —32 codes for $n = 5$, 1028 codes for $n = 10$. The error seems to be bounded by $\lceil \frac{n}{2} \rceil$. For a given m , c_i —the i^{th} coordinate of \mathbf{c} —is randomly assigned a value from the m evenly spaced numbers in the range $[0.1, m/n]$. We set the size of the sampled gradient coordinates set $|\mathcal{D}|$ to $\lfloor n/4 \rfloor$.

unique values (magnitudes) of the gradient coordinates. As detailed in Figure 3, the error can reach $\lceil n/2 \rceil$. This is a big mismatch, especially if we recall the Hamming distance’s range is $[0, n]$. The negative impact of this on the Hamming search strategy by Maurer (2009) was verified empirically in Figure 4. We considered the simplest case where Maurer’s was given access to the noisy Hamming oracle $\hat{\mathcal{O}}$ in a setup similar to the one outlined in Figure 3, with $n = 80$, $|\mathcal{D}| = n/4 = 20$, $m \in \{1, 2\}$, and the hidden code $\mathbf{q}^* = [+1, \dots, +1]$. To account for the randomness in constructing \mathcal{D} , we ran 30 independent runs and plot the average Hamming distance (with confidence bounds) over Maurer’s queries. In Figure 4 (a), $m = 1$ which corresponds to exact estimation $\hat{\mathcal{O}} = \mathcal{O}$, Maurer’s spends 21 queries to construct \mathcal{D} and terminates one query afterwards with the true binary code \mathbf{q}^* , achieving a query ratio of 21/80. On the other hand, when we set $m = 2$ in Figure 4 (b); Maurer’s returns a 4-Hamming-distance away solution from the true binary code \mathbf{q}^* after 51 queries. This is not bad for an 80-bit long code. However, this is in a tightly controlled setup where the gradient magnitudes are just one of two values. To be studied further is the bias/variance decomposition of the returned solution and the corresponding query ratio. We leave this investigation for future work.

3.2 Approach 2: Optimism in the Face of Uncertainty

In the previous approach, we considered the approximated Hamming distance (Eq. 12) as a surrogate for the formal optimization objective (Eq. 4) of the gradient sign estimation problem. We found that current Hamming search strategies are not robust to approximation error. In this approach, we consider maximizing the directional derivative (Eq. 5) as our

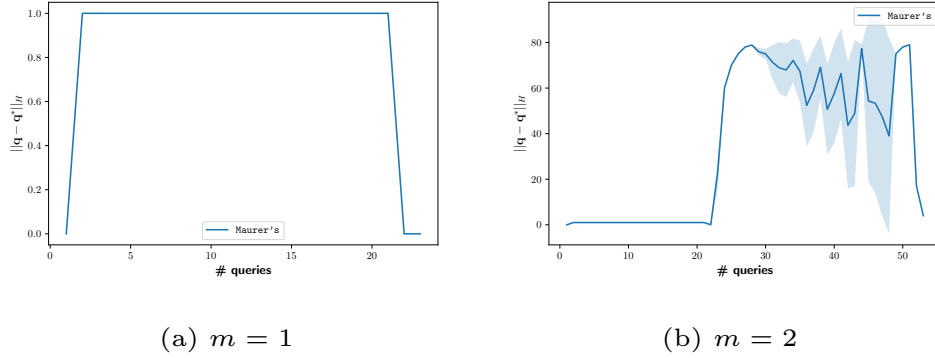


Figure 4: Performance of **Maurer's** on the noisy Hamming oracle $\hat{\mathcal{O}}$. The setup is similar to that of Figure 3, with $n = 80$ and $m \in \{1, 2\}$.

formal objective of the gradient sign estimation problem. Formally, we treat the problem as a binary black-box optimization over the 2^n hypercube vertices, which correspond to all possible sign vectors. This is significantly worse than $O(n)$ of the continuous optimization view. Nevertheless, the rationale here is that we do not need to solve Eq. 5 to optimality (recall Figure 1); we rather need a fast convergence to a suboptimal but *adversarially helpful* sign vector \mathbf{q} . In addition, the continuous optimization view often employs an iterative scheme of T steps within the perturbation ball $B_p(\mathbf{x}, \epsilon)$, calling the *gradient estimation routine* in every step leading to a search complexity of nT . In our setup, we use the best obtained solution for Eq. 5 so far in a similar fashion to the noisy FGSM of Figure 1. In other words, our *gradient sign estimation routine* runs at the top level of our adversarial example generation procedure instead of calling it as a subroutine. In this and the next approach, we address the following question: *how do we solve Eq. 5?*

Optimistic methods, i.e., methods that implement the optimism in the face of uncertainty principle have demonstrated a theoretical as well as empirical success when applied to black-box optimization problems (Al-Dujaili and Suresh, 2017, 2018; Munos, 2011). Such a principle finds its foundations in the machine learning field addressing the exploration vs. exploitation dilemma, known as the multi-armed bandit problem. Within the context of function optimization, optimistic approaches formulate the complex problem of optimizing an arbitrary black-box function g (e.g., Eq. 5) over the search space (\mathcal{H} in this paper) as a hierarchy of simple bandit problems (Kocsis and Szepesvári, 2006) in the form of space-partitioning tree search \mathcal{T} . At step t , the algorithm optimistically expands a leaf node (partitions the corresponding subspace) from the set of leaf nodes \mathcal{L}_t that may contain the global optimum. The i^{th} node at depth h , denoted by (h, i) , corresponds to the subspace/cell $\mathcal{H}_{h,i}$ such that $\mathcal{H} = \cup_{0 \leq i < K^h} \mathcal{H}_{h,i}$. To each node (h, i) , a representative point $\mathbf{q}_{h,i} \in \mathcal{H}_{h,i}$ is assigned, and the value of the node (h, i) is set to $g(\mathbf{q}_{h,i})$. See Figure 6 for an example of a space-partitioning tree \mathcal{T} of \mathcal{H} , which will be used in our second approach to estimate the gradient sign vector.

Under some assumptions on the optimization objective and the hierarchical partitioning \mathcal{T} of the search space, optimistic methods enjoy a finite-time bound on their *regret* R_t defined

as

$$R_t = g(\mathbf{q}^*) - g(\mathbf{q}(t)) , \quad (13)$$

where $\mathbf{q}(t)$ is the best found solution by the optimistic method after t steps. The challenge is how to align the search space such that these assumptions hold. In the following, we show that these assumptions can be satisfied for our optimization objective (Eq. 5). In particular, when $g(\mathbf{q})$ is the directional derivative function $D_{\mathbf{q}}L(\mathbf{x}, y)$, and \mathcal{H} 's vertices are aligned on a 1-dimensional line according to the Gray code ordering, then we can construct an optimistic algorithm with a finite-time bound on its regret. To demonstrate this, we adopt the Simultaneous Optimistic Optimization framework by Munos (2011) and the assumptions therein.

For completeness, we reproduce Munos (2011)'s basic definitions and assumptions with respect to our notation. At the same time we show how the gradient sign estimation problem (Eq. 5) satisfies them based on the second property of the directional derivative as follows.

Definition 2 (Semi-metric) We assume that $\kappa : \mathcal{H} \times \mathcal{H} \rightarrow \mathbb{R}^+$ is such that for all $\mathbf{p}, \mathbf{q} \in \mathcal{H}$, we have $\kappa(\mathbf{p}, \mathbf{q}) = \kappa(\mathbf{q}, \mathbf{p})$ and $\kappa(\mathbf{p}, \mathbf{q}) = 0$ if and only if $\mathbf{p} = \mathbf{q}$.

Definition 3 (Near-optimality dimension) The near-optimal dimension is the smallest $d \geq 0$ such that there exists $C > 0$ such that for any $\varepsilon > 0$, the maximal number of disjoint κ -balls of radius $v\varepsilon$ and center in \mathcal{H}_ε is less than $C\varepsilon^{-d}$.

Property 2 (Local smoothness of $D_{\mathbf{q}}L(\mathbf{x}, y)$) For any input/label pair (\mathbf{x}, y) , there exists at least a global optimizer $\mathbf{q}^* \in \mathcal{H}$ of $D_{\mathbf{q}}L(\mathbf{x}, y)$ (i.e., $D_{\mathbf{q}^*}L(\mathbf{x}, y) = \sup_{\mathbf{q} \in \mathcal{H}} D_{\mathbf{q}}L(\mathbf{x}, y)$) and for all $\mathbf{q} \in \mathcal{H}$,

$$D_{\mathbf{q}^*}L(\mathbf{x}, y) - D_{\mathbf{q}}L(\mathbf{x}, y) \leq \kappa(\mathbf{q}, \mathbf{q}^*) .$$

Refer to Figure 5 for a pictorial proof of Property 2.

Assumption 1 (Bounded diameters) There exists a decreasing sequence $\omega(h) > 0$, such that for any depth $0 \leq h < n$, for any cell $\mathcal{H}_{h,i}$ of depth h , we have $\sup_{\mathbf{q} \in \mathcal{H}_{h,i}} \kappa(\mathbf{q}_{h,i}, \mathbf{q}) \leq \omega(h)$.

To see how Assumption 1 is met, refer to Figure 6.

Assumption 2 (Well-shaped cells) There exists $v > 0$ such that for any depth $0 \leq h < n$, any cell $\mathcal{H}_{h,i}$ contains a κ -ball of radius $v\omega(h)$ centered in $\mathbf{q}_{h,i}$.

To see how Assumption 2 is met, refer to Figure 6. With the above assumptions satisfied, we propose the Gray-code Optimistic Optimization (G00), which is an instantiation of (Munos, 2011, Algorithm 2) tailored to our optimization problem (Eq. 5) over a 1-dimensional alignment of \mathcal{H} using the Gray code ordering. The pseudocode is outlined in Algorithm 1. The following theorem bounds G00's regret.

Theorem 3 Regret Convergence of G00 Let us write $h(t)$ the smallest integer h such that

$$Ch_{\max}(t) \sum_{l=0}^h \omega(l)^{-d} + 1 \geq t . \quad (14)$$

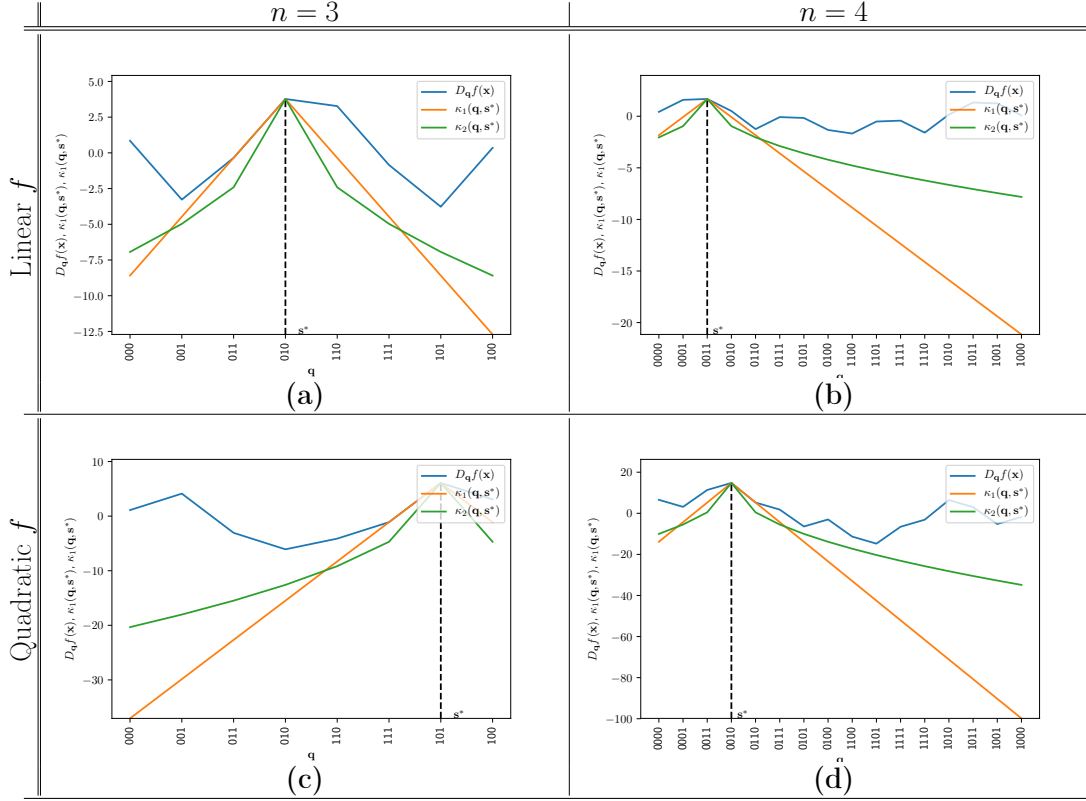


Figure 5: The directional derivative $D_{\mathbf{q}}f(\mathbf{x})$ of some function f at a point \mathbf{x} in the direction of a binary vector $\mathbf{q} \in \mathcal{H} \equiv \{-1, +1\}^n$ is locally smooth around the gradient sign vector, $\mathbf{q}^* = \text{sign}(\nabla_{\mathbf{x}}f(\mathbf{x})) \in \mathcal{H}$, when \mathcal{H} is ordered over one coordinate as a sequence of Gray codes. The plots show the local smoothness property—with two semi-metrics $\kappa_1(\cdot, \cdot)$ and $\kappa_2(\cdot, \cdot)$ —of the directional derivative of functions f of the form $\mathbf{c}^T \mathbf{x}$ and $\mathbf{x}^T \mathbf{Q} \mathbf{x}$ for $n \in \{3, 4\}$, as tabulated in Plots (a), (c) and (b, d), respectively. The local smoothness is evident as $D_{\mathbf{q}^*}f(\mathbf{x}) - D_{\mathbf{q}}f(\mathbf{x}) \leq \kappa_1(\mathbf{q}, \mathbf{q}^*)$ and $D_{\mathbf{q}^*}f(\mathbf{x}) - D_{\mathbf{q}}f(\mathbf{x}) \leq \kappa_2(\mathbf{q}, \mathbf{q}^*)$ for all $\mathbf{q} \in \mathcal{H}$. The semi-metrics $\kappa_1(\mathbf{q}, \mathbf{q}^*)$ and $\kappa_2(\mathbf{q}, \mathbf{q}^*)$ have the form $K|\text{rank}_{\text{Gray}}(\mathbf{q}) - \text{rank}_{\text{Gray}}(\mathbf{q}^*)|^\alpha$, where $\text{rank}_{\text{Gray}}(\cdot)$ refers to the rank of an n -binary code in the Gray ordering of n -binary codes (e.g., $\text{rank}_{\text{Gray}}([-1, -1, +1, -1]) = 4$), $K > 0$, and $\alpha > 0$. With this property at hand, we employ the optimism in the face of uncertainty principle in G00 to maximize $D_{\mathbf{q}}f(\mathbf{x})$ over \mathcal{H} . For legibility, we replaced -1 with 0 when enumerating \mathcal{H} on the x-axis.

Then, with $g(\mathbf{q}) = D_{\mathbf{q}}L(\mathbf{x}, y)$, the regret of G00 (Algorithm 1) is bounded as

$$R_t \leq \omega(\min(h(t), h_{\max}(t) + 1))$$

Proof We have showed that our objective function (Eq. 5) and the hierarchical partitioning of \mathcal{H} following the Gray code ordering confirm to Property 2 and Assumptions 1 and 2. The $+1$ term in Eq. 14 is to accommodate the evaluation of node $(n, 0)$ before growing the space-partitioning tree \mathcal{T} —see Figure 6. The rest follows from the proof of (Munos, 2011, Theorem 2). \blacksquare

Algorithm 1: Gray-code Optimistic Optimization (G00)

Input : $g : \mathcal{H} \rightarrow \mathbb{R}$: the black-box linear function to be maximized over the binary hypercube $\mathcal{H} \equiv \{-1, +1\}^n$

Initialization: Set $t = 1$, $\mathcal{T}_t = \{(0, 0)\}$ (root node). Align \mathcal{H} over \mathcal{T}_t using the Gray code ordering.

```

1 while true do
2    $v_{max} \leftarrow -\infty$ 
3   for  $h = 0$  to  $\min(\text{depth}(\mathcal{T}_t), h_{max}(t))$  do
4     Among all leaves  $(h, j) \in \mathcal{L}_t$  of depth  $h$ , select
                                      $(h, i) \in \arg \max_{(h,j) \in \mathcal{L}_t} g(\mathbf{q}_{h,i})$ 
5     if  $g(\mathbf{q}_{h,i}) \geq v_{max}$  then
6       Expand this node: add to  $\mathcal{T}_t$  the two children  $(h+1, i_k)_{1 \leq k \leq 2}$ 
7        $v_{max} \leftarrow g(\mathbf{q}_{h,i})$ 
8        $t \leftarrow t + 1$ 
9       if query budget is exhausted then
10        return the best found solution  $\mathbf{q}(t)$ .
```

Despite being theoretically-founded, G00 is slow in practice. This is expected since it is a global search technique that considers all the 2^n vertices of the n -dimensional hypercube \mathcal{H} . Recall that we are looking for adversarially helpful solution \mathbf{q} that may not be necessarily optimal. To this end, we consider the *separability* property of the directional derivative, a more useful property than its local smoothness as described in our third approach next.

3.3 Approach 3: Divide & Conquer

Based on the definition of the directional derivative (Eq. 2), we state the following property.

Property 3 (Separability of $D_{\mathbf{q}}L(\mathbf{x}, y)$) *The directional derivative $D_{\mathbf{q}}L(\mathbf{x}, y)$ of the loss function L at an input/label pair (\mathbf{x}, y) in the direction of a binary code \mathbf{q} is separable. That is,*

$$\max_{\mathbf{q} \in \mathcal{H}} D_{\mathbf{q}}L(\mathbf{x}, y) = \max_{\mathbf{q} \in \mathcal{H}} \mathbf{q}^T \mathbf{g}^* = \sum_{i=1}^n \max_{q_i \in \{0,1\}} q_i g_i^* \quad (15)$$

Instead of considering the 2^n search space (Section 3.2), we employ the above property in a divide-and-conquer search which we refer to as **SignHunter**. As outlined in Algorithm 2, the technique starts with a random guess of the sign vector \mathbf{q}_1 . It then proceeds to flip the sign of all the coordinates to get a new sign vector \mathbf{q}_2 , and revert the flips if the loss oracle returned a value $L(\mathbf{x} + \delta \mathbf{q}_2, y)$ (or equivalently the directional derivative) less than the best obtained so far $L(\mathbf{x} + \delta \mathbf{q}_1, y)$. **SignHunter** applies the same rule to the first half of the coordinates, the second half, the first quadrant, the second quadrant, and so on. For a search space of dimension n , **SignHunter** needs $2^{\lceil \log(n)+1 \rceil} - 1$ sign flips to complete its search. If

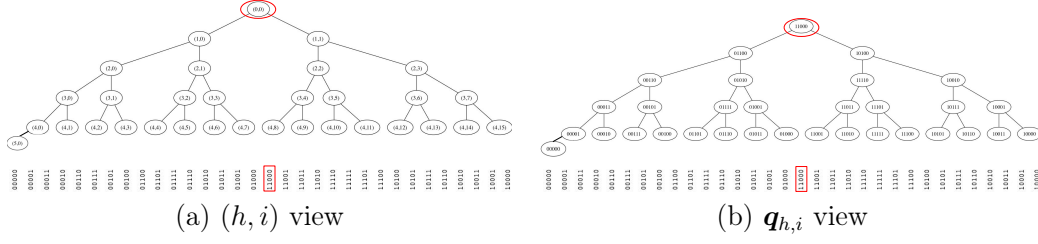


Figure 6: Illustration of the proposed Gray-ordering based partitioning (fully expanded) tree \mathcal{T} of the search space $\mathcal{H} = \{-1, +1\}^n$ —with $n = 5$ —used in the Gray-code Optimistic Optimization (GOO). The plots are two different views of the same tree. Plot (a) displays the node name (h, i) , while Plot (b) shows its representative binary code $q_{h,i} \in \mathcal{H}$. For brevity, we replaced -1 s with 0s. The red oval and rectangle highlights the tree’s root and its corresponding binary code, respectively. Consider the node $(2, 1)$ whose representative code is $q_{2,1} = [-1, +1, -1, +1, -1]$ and its corresponding subspace $\mathcal{H}_{2,1} = \{q_{2,1}, q_{3,2}, q_{3,3}, q_{4,4}, q_{4,5}, q_{4,6}, q_{4,7}\}$. The same reasoning applies to the rest of the nodes. To maintain a valid binary partition tree, one can ignore the anomaly leaf node $(5, 0)$, this corresponds to the code $q_{5,0} = [-1, -1, -1, -1, -1]$, which in practice can be evaluated prior to building the tree. Let us consider the nodes at depth $h = 2$, observe that for all $i \in \{0, 1, 2, 3\}$ 1) $|\mathcal{H}_{2,i}| = 7$; 2) $q_{2,i}$ is centered around the other 6 members of $\mathcal{H}_{2,i}$ in the Gray code ordering; and that 3) $\mathcal{H}_{2,i}$ constitutes a contiguous block of codes along the 1-dimensional alignment shown below the tree. Thus, it suffices to define a semi-metric based on the corresponding indices of the codes along this alignment. For a given depth h , the index of any code $q \in \mathcal{H}_{h,i}$ is at most $\omega(h) = \sup_j |\mathcal{H}_{h+1,j}|$, which establishes Assumption 2. Assumption 3 follows naturally from the fact that nodes at a given depth h partition the search space \mathcal{H} equally (e.g., $|\mathcal{H}_{2,i}| = 7$ for all i).

the query budget is not exhausted by then, one can update \mathbf{x} with the recovered signs and restart the procedure at the updated point with a new starting code q_1 (s in Algorithm 2). In the next theorem, we show that **SignHunter** is guaranteed to perform at least as well as the Fast Gradient Sign Method FGSM after $O(2n)$ oracle queries.

Theorem 4 (Optimality of SignHunter) *Given $2^{\lceil \log(n)+1 \rceil}$ queries, **SignHunter** is at least as effective as FGSM (Goodfellow et al., 2015) in crafting adversarial examples.*

Proof The i th coordinate of the gradient sign vector can be recovered as outlined in Eq. 9 which takes 2 queries. From the definition of **SignHunter**, this is carried out for all the n coordinates after $2^{\lceil \log(n)+1 \rceil}$ queries. That is, the gradient sign vector is fully recovered after $2^{\lceil \log(n)+1 \rceil}$ queries, and therefore one can employ the FGSM attack to craft adversarial examples. \blacksquare

Theorem 4 provides an upper bound on the number of queries required for **SignHunter** to recover the gradient sign bits, and perform as well as FGSM. In practice (as will be shown in our experiments), **SignHunter** crafts adversarial examples with a fraction of this upper bound. Note that one could recover the gradient sign vector with $n + 1 < O(2n)$ queries by starting with an arbitrary sign vector and flipping its bits sequentially. Nevertheless, **SignHunter** incorporates the $O(2n)$ queries in a framework of majority voting to recover as

Algorithm 2: SignHunter

Input : $g : \mathcal{H} \rightarrow \mathbb{R}$: the black-box linear function to be maximized over the binary hypercube $\mathcal{H} \equiv \{-1, +1\}^n$

```

1 def init( $g$ ) :
2      $i \leftarrow 0$ 
3      $h \leftarrow 0$ 
4      $g \leftarrow g$ 
5      $\mathbf{s} \sim \mathcal{U}(\mathcal{H})$ 
6      $\text{done} \leftarrow \text{false}$ 
7      $g_{\text{best}} \leftarrow g(\mathbf{s})$ 

8 def is_done() :
9     return done

10 def step() :
11      $\text{chunk\_len} \leftarrow \lceil n/2^h \rceil$ 
12     flip the bits of  $\mathbf{s}$  indexed from  $i \cdot \text{chunk\_len}$  till  $(i+1) \cdot \text{chunk\_len}$ 
13     if  $g(\mathbf{s}) \geq g_{\text{best}}$ :
14          $g_{\text{best}} \leftarrow g(\mathbf{s})$ 
15     else:
16         flip back the bits of  $\mathbf{s}$  indexed from  $i \cdot \text{chunk\_len}$  till  $(i+1) \cdot \text{chunk\_len}$ 
17     increment  $i$ 
18     if  $i == 2^h$ :
19          $i \leftarrow 0$ 
20     increment  $h$ 
21     if  $h == \lceil \log_2(n) \rceil + 1$ :
22          $\text{done} \leftarrow \text{true}$ 

23 def get_current_sign_estimate() :
24     return  $\mathbf{s}$ 
```

many sign bits as possible with as few queries as possible. Consider the case where all the gradient coordinates have the same magnitude—the $m = 1$ case in Figure 3. If we start with a random sign vector whose Hamming distance to the optimal sign vector \mathbf{q}^* is $n/2$: agreeing with \mathbf{q}^* in the first half of coordinates. In this case, **SignHunter** needs just *four* queries to recover the entire sign vector, whereas the sequential bit flipping would require $n + 1$ queries.

Moreover, **SignHunter** is amenable to parallel hardware architecture and thus can carry out attacks in batches more efficiently, compared to the previous presented approaches. We tested both **G00** and **SignHunter** (along with **Maurer’s** and **Elimination**) on a set of toy problems and found that **SignHunter** performs significantly better than **G00**, while **Maurer’s** and **Elimination** were sensitive to the approximation error—see Figure 7. For these reasons, in our experiments on the real datasets **MNIST**, **CIFAR10**, **IMAGENET**; we

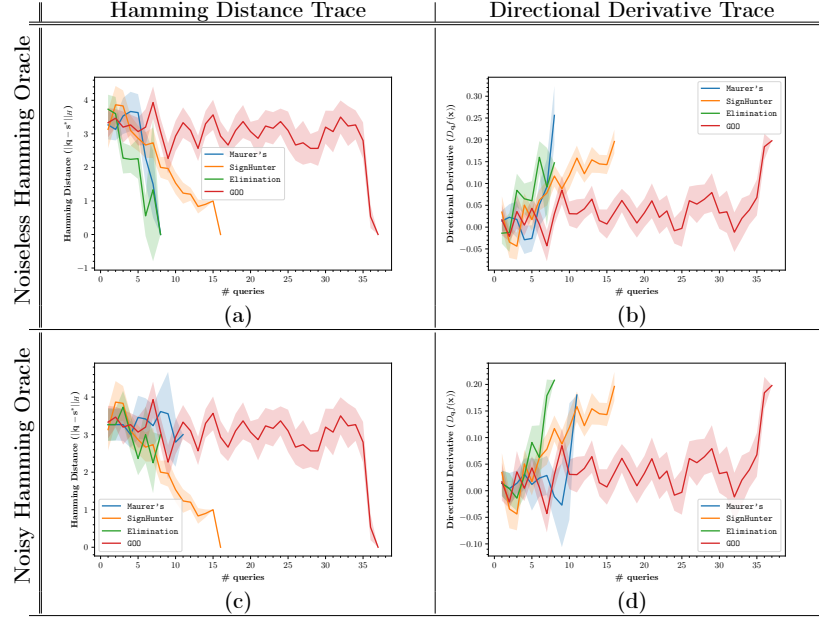


Figure 7: *Noiseless vs. Noisy Hamming Oracle*: The trace of the Hamming distance (first column, where the lower the trace the better) and directional derivative (second column, where the higher the trace the better) values of **Elimination** and **Maurer’s** queries, when given access to a noiseless/ideal (first row) and noisy Hamming oracles (second row)—through a directional derivative approximation as discussed in Section ?? of the main paper—for a synthetic function f of the form $\mathbf{x}^T Q \mathbf{x}$ with $n = 7$. We expect the traces to go up and down as they explore the 2^n search space. The end of an algorithm’s trace represents the value of the Hamming distance (directional derivative) for the first column (for the second column) at the algorithm’s solution. For comparison, we also plot **G00** and **SignHunter**’s traces. Note that the performance of **G00** and **SignHunter** is the same in both noiseless and noisy cases as both algorithms operate directly on the directional derivative approximation rather than the noiseless/noisy Hamming oracle. In the case of noiseless Hamming oracle, both **Elimination** and **Maurer’s** finds the optimal vector $\mathbf{q}^* \in \mathcal{H} \equiv \{-1, +1\}^7$ with $\#$ queries ≤ 7 —their traces end at most at 8 just to show that the algorithm’s solution achieves a zero Hamming distance as shown in Plot (a), which corresponds to the maximum directional derivative in Plot (b). With a noisy Hamming oracle, these algorithm break as shown in Plots (c) and (d): taking more than n queries and returning sub-optimal solutions—e.g., **Maurer’s** returns on average a three-Hamming-distance solution. On the other hand, **G00** and **SignHunter** achieve a zero Hamming distance in both cases at the expense of being less query efficient. While being theoretically-founded, **G00** is slow as it employs a global search over the 2^n space. Despite **SignHunter**’s local search, it converges to the optimal solution after 2×7 queries in accordance with Theorem 4. The solid curves indicate the corresponding averaged trace surrounded by a 95%-confidence bounds using 30 independent runs. For convenience, we plot the symmetric bounds where in fact they should be asymmetric in Plots (a) and (c) as the Hamming distance’s range is \mathbb{Z}_0^+ .

opted for **SignHunter** as our algorithm of choice to estimate the gradient sign in crafting black-box adversarial attacks as outlined in Algorithm 3.

Algorithm 3: Black-Box Adversarial Example Generation with **SignHunter**

Input :

\mathbf{x}_{init} : input to be perturbed,
 y_{init} : \mathbf{x}_{init} 's true label,
 $B_p(\cdot, \epsilon)$: ℓ_p perturbation ball of radius ϵ ,
 L : loss function of the neural net under attack

1 $\delta \leftarrow \epsilon$
2 $\mathbf{x}_o \leftarrow \mathbf{x}_{init}$ // Adversarial input to be constructed
3 Define the function g as

$$g(\mathbf{q}) = \frac{L(\mathbf{x}_o + \delta \mathbf{q}, y_{init}) - L(\mathbf{x}_o, y_{init})}{\delta}$$

4 *SignHunter*.init(g)
5 // $C(\cdot)$ returns top class
6 **while** $C(\mathbf{x}) = y_{init}$ **do**
7 *SignHunter*.step()
8 $\mathbf{s} \leftarrow \text{SignHunter.get_current_sign_estimate}()$
9 $\mathbf{x} \leftarrow \Pi_{B_p(\mathbf{x}_{init}, \epsilon)}(\mathbf{x}_o + \delta \mathbf{s})$
10 **if** *SignHunter.is_done*() **then**
11 $\mathbf{x}_o \leftarrow \mathbf{x}$
12 Define the function g as

$$g(\mathbf{q}) = \frac{L(\mathbf{x}_o + \delta \mathbf{q}, y_{init}) - L(\mathbf{x}_o, y_{init})}{\delta}$$

13 *SignHunter*.init(g)
14 **return** \mathbf{x}

4. Experiments

In this section, we evaluate **SignHunter** and compare it with established algorithms from the literature: **Z0-SignSGD** (Liu et al., 2019), **NES** (Ilyas et al., 2018), and **Bandits_{TD}** (Ilyas et al., 2019) in terms of their effectiveness in crafting untargeted black-box adversarial examples. Both ℓ_∞ and ℓ_2 threat models are considered on the **MNIST**, **CIFAR10**, and **IMAGENET** datasets.

4.1 Experiments Setup

Our experiment setup is similar to (Ilyas et al., 2019). Each attacker is given a budget of 10,000 oracle queries per attack attempt and is evaluated on 1000 images from the test sets of **MNIST**, **CIFAR10**, and **IMAGENET**. We did not find a standard practice of setting the perturbation bound ϵ , arbitrary bounds were used in several papers. We set the perturbation bounds based on the following.

- For the ℓ_∞ threat model, we use (Madry et al., 2017)’s bound for **MNIST** and (Ilyas et al., 2019)’s bounds for both **CIFAR10** and **IMAGENET**.
- For the ℓ_2 threat model, (Ilyas et al., 2019)’s bound is used for **IMAGENET**. **MNIST**’s bound is set based on the sufficient distortions observed in (Liu et al., 2019), which are smaller than the one used in (Madry et al., 2017). We use the observed bound in (Cohen et al., 2019) for **CIFAR10**.

We show results based on standard models. For **MNIST** and **CIFAR10**, the naturally trained models from (Madry et al., 2017)’s **MNIST**⁷ and **CIFAR10**⁸ challenges are used. For **IMAGENET**, the *Inception-V3* model from TensorFlow is used.⁹ The loss oracle represents the cross-entropy loss of the respective model. General setup of the experiments is summarized in Table 2 in Appendix B.

4.2 Hyperparameters Setup

To ensure a fair comparison among the considered algorithms, we did our best in tuning their hyperparameters. Initially, the hyperparameters were set to the values reported by the corresponding authors, for which we observed suboptimal performance. This can be attributed to either using a different software framework (e.g., TensorFlow vs. PyTorch), models, or the way the model’s inputs are transformed (e.g., some models take pixel values to be in the range $[0, 1]$ while others are built for $[0, 255]$). We made use of a synthetic concave loss function to tune the algorithms’ parameters for each dataset \times perturbation constraint combination. The performance curves on the synthetic loss function using the tuned values of the hyperparameters did show consistency with the reported results from the literature. For instance, we noted that **Z0-SignSGD** converges faster than **NES**. Further, **Bandits_{TD}** outperformed the rest of the algorithms towards the end of query budget. That said, we invite the community to provide their best tuned attacks. Note that **SignHunter** does not have any hyperparameters to tune. The finite difference probe δ for **SignHunter** is set to the perturbation bound ϵ because this perturbation is used for both computing the finite difference and crafting the adversarial examples—see Line 9 in Algorithm 2. This parameter-free setup of **SignHunter** offers a robust edge over the state-of-the-art black-box attacks, which often require expert knowledge to carefully tune their parameters as discussed above. More details on the hyperparameters setup can be found in Appendix B.

4.3 Results

Figures 8 and 9 show the trade-off between the success (evasion) rate and the mean number of queries (of the successful attacks) needed to generate an adversarial example for the **MNIST**, **CIFAR10**, and **IMAGENET** classifiers in the ℓ_∞ and ℓ_2 perturbation constraints, respectively. In other words, these figures indicate the average number of queries required for a desired success rate. Tabulated summary of these plots can be found in Appendix D, namely Tables 7, 8, and 9. Furthermore, we plot the classifier loss and the gradient

⁷https://github.com/MadryLab/mnist_challenge

⁸https://github.com/MadryLab/cifar10_challenge

⁹https://github.com/tensorflow/tensorflow/blob/master/tensorflow/contrib/slim/python/slim/nets/inception_v3_test.py

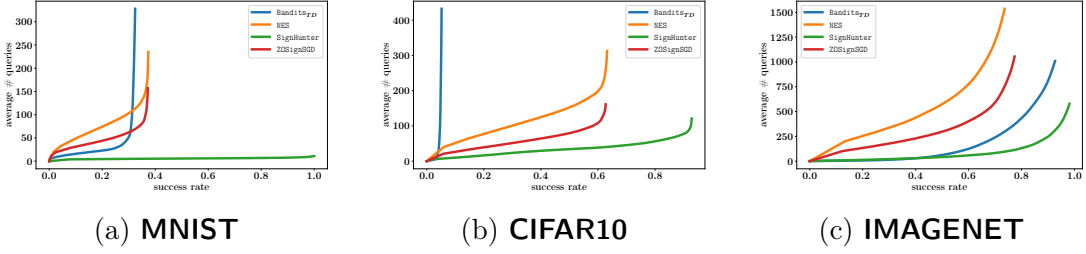


Figure 8: Performance of black-box attacks in the ℓ_∞ perturbation constraint. The plots show the average number of queries used per successful image for each attack when reaching a specified success rate.

estimation quality (in terms of Hamming distance and Cosine similarity) averaged over all the images as a function of the number of queries used as shown in Figures 14, 15, and 16 in Appendix D. Based on the results, we observe the following:

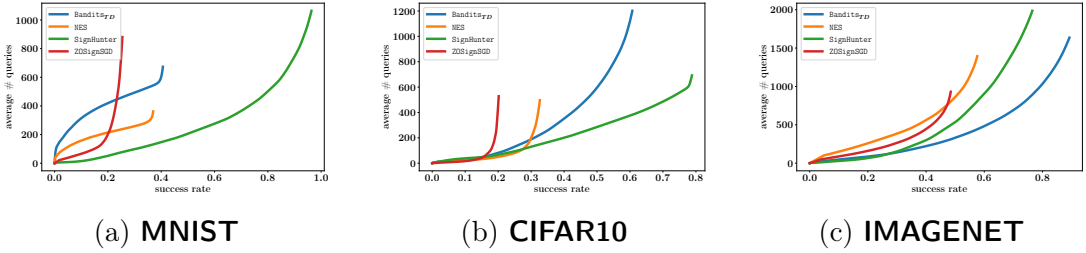


Figure 9: Performance of black-box attacks in the ℓ_2 perturbation constraint. The plots show the average number of queries used per successful image for each attack when reaching a specified success rate.

- For any given success rate, **SignHunter** dominates the previous state of the art approaches in all settings except the **IMAGENET** ℓ_2 setup,¹⁰ where **BanditsTD** shows a better query efficiency when the desired success rate is greater than or equal ~ 0.35 .
- **SignHunter** is remarkably efficient in the ℓ_∞ setup (e.g., achieving a **100%** evasion using—on average—just **12** queries per image against the **MNIST** classifier!). Its performance degrades—yet, still outperforms the rest, most of the time—in the ℓ_2 setup. This is expected, since **SignHunter** perturbs all the coordinates with the same magnitude and the ℓ_2 perturbation bound for all the datasets in our experiments is set such that $\epsilon_2/\sqrt{n} \ll \epsilon_\infty$ as shown in Table 2. Take the case of **MNIST** ($n = 28 \times 28$), where $\epsilon_\infty = 0.3$ and $\epsilon_2 = 3$. For **SignHunter**, the ℓ_2 setup is equivalent to an ℓ_∞ perturbation bound of $3/28 \approx 0.1$. The employed ℓ_2 perturbation bounds give the state of the art—continuous optimization based—approaches more perturbation options. For

¹⁰To be accurate, all the algorithms are comparable in the **CIFAR10** ℓ_2 setup for success rate ≤ 0.3 .

instance, it is possible for **NES** to perturb one pixel in an MNIST image by a magnitude of 3 each; two pixels by a magnitude of 2.1 each; and ten pixels by a magnitude of 0.9 each. On the other hand, the binary optimization view of **SignHunter** limits it to always perturb all 28×28 pixels by a magnitude of 0.1. Despite its less degrees of freedom, **SignHunter** maintains its effectiveness in the ℓ_2 setup. On the other hand, the plots can be viewed as a sensitivity assessment of **SignHunter** as ϵ gets smaller for each dataset.

- The plots verify Theorem 4 when compared with the performance of **FGSM** (Figures 10 and 11 in Appendix A, the noisy **FGSM** at $k = 100\%$) in both ℓ_∞ and ℓ_2 setups for **MNIST** and **CIFAR10**—for **IMAGENET**, $2n = 536,406$ is beyond our query budget of 10,000 queries. For example, **FGSM** has a failure rate of 0.32 for **CIFAR10** ℓ_2 (Figure 11 (b)), while **SignHunter** achieves a failure rate of 0.21 with $692.39 < 2n = 2 \times 3 \times 32 \times 32 = 6144$ queries.
- Incorporating **SignHunter** in an iterative framework of perturbing the data point \mathbf{x} till the query budget is exhausted (Lines 10 to 13 in Algorithm 3) supports the observation in white-box settings that iterative **FGSM**—or Projected Gradient Descent (**PGD**)—is stronger than **FGSM** (Al-Dujaili et al., 2018; Madry et al., 2017). This is evident by the upticks in **SignHunter**’s performance on the **MNIST** ℓ_2 case (Figure 14: classifier’s loss, average Cosine distance, and average Hamming similarity plots), which happens after every iteration (after every other $2 \times 28 \times 28$ queries).
- Plots of the average Hamming similarity capture the quality of the gradient sign estimation in terms of Eq. 4, while plots of the average Cosine similarity capture it in terms of Eq. 5. Both **SignHunter** and **Bandits_{TD}** consistently optimize both objectives. In general, **SignHunter** enjoys a faster convergence especially on the Hamming metric because it is estimating the signs compared to **Bandits_{TD}**’s full gradient estimation. This is highlighted in the **IMAGENET** ℓ_2 setup. Note that once an attack is successful, the gradient sign estimation at that point is used for the rest of the plot. This explains why, in the ℓ_∞ settings, **SignHunter**’s plot does not improve compared to its ℓ_2 counterpart, as most of the attacks are successful in the very first few queries made in the oracle.

Overall, **SignHunter** fails $3.8\times$ less often than the state-of-the-art approaches combined, and spend over all the images (successful and unsuccessful attacks) $2.5\times$ less queries. The number of queries spent is computed as

$$(1 - \text{fail_rate}) * \text{avg_}\#\text{queries} + \text{fail_rate} * 10,000$$

based on Tables 7, 8, and 9.

5. Public MNIST Black-Box Attack Challenge

To complement our results in Section 4, we evaluated **SignHunter**’s effectiveness against *adversarial training*, an effective way to improve the robustness of DNNs (Al-Dujaili et al., 2018; Madry et al., 2017). In particular, we attacked the *secret* model used in the public

MNIST Black-Box Challenge¹¹ using the challenge setup: 10,000 test images with an ℓ_∞ perturbation bound of $\epsilon = 0.3$. Although the secret model is released, we treated as a black-box similar to our experiments in Section 4. There was no specification of maximum query budget, so we set it to half the budget used in Section 4. As shown in Table 1, **SignHunter**'s attacks resulted in the lowest model accuracy of **91.47%**, outperforming all other state-of-the-art attack strategies submitted to the challenge with an average number of queries of **233** per successful attack.

Table 1: Black-Box Leaderboard for the public **MNIST** black-box attack challenge.

Attack	Model Accuracy
SignHunter (Algorithm 3)	91.47%
Xiao et al. (2018)	92.76%
PGD against three independently and adversarially trained copies of the network	93.54%
FGSM on the CW loss for model B from (Tramèr et al., 2017)	94.36%
FGSM on the CW loss for the naturally trained public network	96.08%
PGD on the cross-entropy loss for the naturally trained public network	96.81%
Attack using Gaussian Filter for selected pixels on the adversarially trained public network	97.33%
FGSM on the cross-entropy loss for the adversarially trained public network	97.66%
PGD on the cross-entropy loss for the adversarially trained public network	97.79%

6. Conclusion

In this paper, we studied the problem of generating adversarial examples for neural nets assuming a *black-box* threat model. Motivated by i) the significant empirical effectiveness of gradient sign information; and ii) the low query complexity of recovering a sign vector using a noiseless Hamming distance oracle, we proposed the gradient *sign* estimation problem as the core challenge in crafting adversarial examples, and we formulate it as a *binary black-box optimization problem*: minimizing the Hamming distance to the gradient sign or, equivalently, maximizing the directional derivative.

Approximated by the finite difference of the loss value queries, we examine three properties of the directional derivative of the model's loss in the direction of $\{\pm 1\}^n$ vectors. Based on the first property, the loss oracle can be used as a noisy Hamming distance oracle. We found that current search Hamming search strategies (e.g. Maurer (2009)) are not suitable for such oracles. The second property lets us employ the *optimism in the face of uncertainty principle* in the form of hierarchical bandits. This resulted in **G00**, an optimistic optimization algorithm for binary black-box optimization problems with a finite-time analysis on its regret. However, its query complexity is worse than the continuous optimization setup. The third property of separability helped us devise **SignHunter**, a divide-and-conquer algorithm that is guaranteed to perform *at least* as well as FGSM after $O(2n)$ queries. In practice, **SignHunter** needs a fraction of this number of queries to craft adversarial examples. To verify its effectiveness on real-world datasets, **SignHunter** was compared against the state-of-the-art black-box attacks on neural network models for the **MNIST**, **CIFAR10**, and **IMAGENET** datasets. **SignHunter** yields black-box attacks that are $2.5\times$ more query efficient and $3.8\times$ less failure-prone than the state of the art attacks combined. Moreover, **SignHunter** achieves the highest evasion

¹¹https://github.com/MadryLab/mnist_challenge

rate on a public **MNIST** black-box attack challenge surpassing eight other attacks that are based on transferability and generative adversarial networks.

Current version of **SignHunter** does not exploit any data- or time-dependent priors. With these priors, algorithms such as **Bandits_{TD}** operate on a search space of dimensionality $\sim 36\times$ less than that of **SignHunter** for **IMAGENET**. Besides, early restart techniques are generally used in similar setups. We intend to explore these factors in a future work.

Acknowledgments

This work was supported by the MIT-IBM Watson AI Lab. The authors would like to thank Shashank Srikant for his timely help.

References

- Abdullah Al-Dujaili and Sundaram Suresh. Embedded bandits for large-scale black-box optimization. In *Thirty-First AAAI Conference on Artificial Intelligence*, 2017.
- Abdullah Al-Dujaili and Sundaram Suresh. Multi-objective simultaneous optimistic optimization. *Information Sciences*, 424:159–174, 2018.
- Abdullah Al-Dujaili, Alex Huang, Erik Hemberg, and Una-May O’Reilly. Adversarial deep learning for robust detection of binary encoded malware. In *2018 IEEE Security and Privacy Workshops (SPW)*, pages 76–82. IEEE, 2018.
- Jeremy Bernstein, Yu-Xiang Wang, Kamyar Azizzadenesheli, and Animashree Anandkumar. signSGD: Compressed optimisation for non-convex problems. In Jennifer Dy and Andreas Krause, editors, *Proceedings of the 35th International Conference on Machine Learning*, volume 80 of *Proceedings of Machine Learning Research*, pages 560–569, Stockholmsmässan, Stockholm Sweden, 10–15 Jul 2018. PMLR. URL <http://proceedings.mlr.press/v80/bernstein18a.html>.
- Arjun Nitin Bhagoji, Warren He, Bo Li, and Dawn Song. Exploring the space of black-box attacks on deep neural networks. *arXiv preprint arXiv:1712.09491*, 2017.
- Battista Biggio and Fabio Roli. Wild patterns: Ten years after the rise of adversarial machine learning. *Pattern Recognition*, 84:317–331, 2018.
- Battista Biggio, Iginio Corona, Davide Maiorca, Blaine Nelson, Nedim Šrđić, Pavel Laskov, Giorgio Giacinto, and Fabio Roli. Evasion attacks against machine learning at test time. In *Joint European conference on machine learning and knowledge discovery in databases*, pages 387–402. Springer, 2013.
- Nicholas Carlini and David Wagner. Towards evaluating the robustness of neural networks. In *2017 IEEE Symposium on Security and Privacy (SP)*, pages 39–57. IEEE, 2017.
- Pin-Yu Chen, Huan Zhang, Yash Sharma, Jinfeng Yi, and Cho-Jui Hsieh. Zoo: Zeroth order optimization based black-box attacks to deep neural networks without training substitute

- models. In *Proceedings of the 10th ACM Workshop on Artificial Intelligence and Security*, pages 15–26. ACM, 2017.
- Jeremy Cohen, Elan Rosenfeld, and J. Zico Kolter. Certified adversarial robustness via randomized smoothing. *arXiv:1902.02918v1*, 2019.
- Ian Goodfellow, Jonathon Shlens, and Christian Szegedy. Explaining and harnessing adversarial examples. In *International Conference on Learning Representations*, 2015. URL <http://arxiv.org/abs/1412.6572>.
- Jamie Hayes and George Danezis. Machine learning as an adversarial service: Learning black-box adversarial examples. *CoRR*, abs/1708.05207, 2017.
- Alex Huang, Abdullah Al-Dujaili, Erik Hemberg, and Una-May O’Reilly. On visual hallmarks of robustness to adversarial malware. In *2018 IJCAI Workshop on Interpretable & Reasonable Deep Learning and its Applications (IReDLiA)*, 2018.
- Andrew Ilyas, Logan Engstrom, Anish Athalye, and Jessy Lin. Black-box adversarial attacks with limited queries and information. In Jennifer Dy and Andreas Krause, editors, *Proceedings of the 35th International Conference on Machine Learning*, volume 80 of *Proceedings of Machine Learning Research*, pages 2137–2146, Stockholmsmässan, Stockholm Sweden, 10–15 Jul 2018. PMLR. URL <http://proceedings.mlr.press/v80/ilyas18a.html>.
- Andrew Ilyas, Logan Engstrom, and Aleksander Madry. Prior convictions: Black-box adversarial attacks with bandits and priors. In *International Conference on Learning Representations*, 2019. URL <https://openreview.net/forum?id=BkMiWhR5K7>.
- Levente Kocsis and Csaba Szepesvári. Bandit based monte-carlo planning. In *European conference on machine learning*, pages 282–293. Springer, 2006.
- Alexey Kurakin, Ian J. Goodfellow, and Samy Bengio. Adversarial machine learning at scale. 2017. URL <https://arxiv.org/abs/1611.01236>.
- Sijia Liu, Pin-Yu Chen, Xiangyi Chen, and Mingyi Hong. signSGD via zeroth-order oracle. In *International Conference on Learning Representations*, 2019. URL <https://openreview.net/forum?id=BJe-DsC5Fm>.
- Yanpei Liu, Xinyun Chen, Chang Liu, and Dawn Song. Delving into transferable adversarial examples and black-box attacks. *arXiv preprint arXiv:1611.02770*, 2016.
- Aleksander Madry, Aleksandar Makelov, Ludwig Schmidt, Dimitris Tsipras, and Adrian Vladu. Towards deep learning models resistant to adversarial attacks. *arXiv preprint arXiv:1706.06083*, 2017.
- Peter M Maurer. A search strategy using a hamming-distance oracle. 2009.
- Seyed-Mohsen Moosavi-Dezfooli, Alhussein Fawzi, and Pascal Frossard. Deepfool: a simple and accurate method to fool deep neural networks. In *Proceedings of the IEEE Conference on Computer Vision and Pattern Recognition*, pages 2574–2582, 2016.

- Rémi Munos. Optimistic optimization of a deterministic function without the knowledge of its smoothness. In *Advances in neural information processing systems*, pages 783–791, 2011.
- Nina Narodytska and Shiva Prasad Kasiviswanathan. Simple black-box adversarial attacks on deep neural networks. In *CVPR Workshops*, volume 2, 2017.
- Blaine Nelson, Benjamin IP Rubinstein, Ling Huang, Anthony D Joseph, Steven J Lee, Satish Rao, and JD Tygar. Query strategies for evading convex-inducing classifiers. *Journal of Machine Learning Research*, 13(May):1293–1332, 2012.
- Nicolas Papernot, Patrick McDaniel, Ian Goodfellow, Somesh Jha, Z Berkay Celik, and Ananthram Swami. Practical black-box attacks against machine learning. In *Proceedings of the 2017 ACM on Asia Conference on Computer and Communications Security*, pages 506–519. ACM, 2017.
- Adi Shamir, Itay Safran, Eyal Ronen, and Orr Dunkelman. A simple explanation for the existence of adversarial examples with small hamming distance. *arXiv preprint arXiv:1901.10861*, 2019.
- Florian Tramèr, Alexey Kurakin, Nicolas Papernot, Ian Goodfellow, Dan Boneh, and Patrick McDaniel. Ensemble adversarial training: Attacks and defenses. *arXiv preprint arXiv:1705.07204*, 2017.
- Chun-Chen Tu, Paishun Ting, Pin-Yu Chen, Sijia Liu, Huan Zhang, Jinfeng Yi, Cho-Jui Hsieh, and Shin-Ming Cheng. Autozoom: Autoencoder-based zeroth order optimization method for attacking black-box neural networks. *arXiv preprint arXiv:1805.11770*, 2018.
- Vinay Anant Vaishampayan. Query matrices for retrieving binary vectors based on the hamming distance oracle. *arXiv preprint arXiv:1202.2794*, 2012.
- Chaowei Xiao, Bo Li, Jun-Yan Zhu, Warren He, Mingyan Liu, and Dawn Song. Generating adversarial examples with adversarial networks, 2018. URL <https://openreview.net/forum?id=HknbyQbC->.
- Yun-Bin Zhao. *Sparse optimization theory and methods*. CRC Press, an imprint of Taylor and Francis, Boca Raton, FL, 2018. ISBN 978-1138080942.

Appendix A. Noisy FGSM

This section shows the performance of the noisy FGSM on standard models (described in Section 4) on the **MNIST**, **CIFAR10** and **IMAGENET** datasets. In Figure 10, we consider the ℓ_∞ threat perturbation constraint. Figure 11 reports the performance for the 2 setup. Similar to Ilyas et al. (2019), for each k in the experiment, the top k percent of the signs of the coordinates—chosen either randomly (**random-k**) or by the corresponding magnitude (**top-k**)—are set correctly, and the rest are set to -1 or $+1$ at random. The misclassification rate shown considers only images that were correctly classified (with no adversarial perturbation). In accordance with the models' accuracy, there were 987, 962, and 792 such images for **MNIST**, **CIFAR10**, and **IMAGENET** out of the sampled 1000 images, respectively. These figures also serve as a validation for Theorem 4 when compared to SignHunter's performance shown in Appendix C.

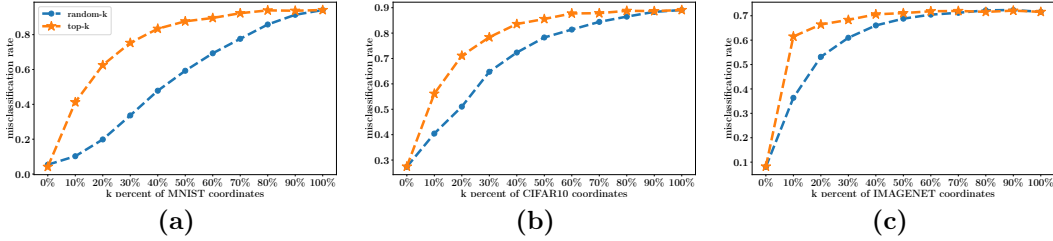


Figure 10: Misclassification rate of three neural nets (for (a) **MNIST**, (b) **CIFAR10**, and (c) **IMAGENET**, respectively) on the *noisy* FGSM's adversarial examples as a function of correctly estimated coordinates of $\text{sign}(\nabla_{\mathbf{x}} f(\mathbf{x}, y))$ on random 1000 images from the corresponding evaluation dataset, with the maximum allowed ℓ_∞ perturbation ϵ being set to 0.3, 12, and 0.05, respectively. Across all the models, estimating the sign of the top 30% gradient coordinates (in terms of their magnitudes) is enough to achieve a misclassification rate of $\sim 70\%$. Note that Plot (c) is similar to Ilyas et al. (2019)'s Figure 1, but it is produced with TensorFlow rather than PyTorch.

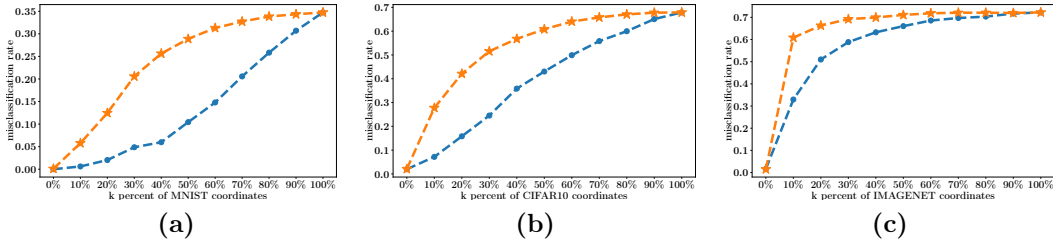


Figure 11: Misclassification rate of three neural nets (for (a) **MNIST**, (b) **CIFAR10**, and (c) **IMAGENET**, respectively) on the *noisy* FGSM's adversarial examples as a function of correctly estimated coordinates of $\text{sign}(\nabla_{\mathbf{x}} f(\mathbf{x}, y))$ on random 1000 images from the corresponding evaluation dataset, with the maximum allowed ℓ_2 perturbation ϵ being set to 3, 127, and 5, respectively. Compared to Figure 10, the performance on **MNIST** and **CIFAR10** drops significantly.

Appendix B. Experiments Setup

This section outlines the experiments setup as follows. Figure 12 shows the performance of the considered algorithms on a synthetic concave loss function after tuning their hyperparameters. A possible explanation of **SignHunter**'s superb performance is that the synthetic loss function is well-behaved in terms of its gradient given an image. That is, most of gradient coordinates share the same sign, since pixels tend to have the same values and the optimal value for all the pixels is the same $\frac{x_{min}+x_{max}}{2}$. Thus, **SignHunter** will recover the true gradient sign with as few queries as possible (recall the example in Section 3.3). Moreover, given the structure of the synthetic loss function, the optimal loss value is always at the boundary of the perturbation region. The boundary is where **SignHunter** samples its perturbations. Tables 3, 4, 5, and 6 outline the algorithms' hyperparameters, while Table 2 describes the general setup for the experiments.

Table 2: General setup for all the attacks

Parameter	Value					
	MNIST		CIFAR10		IMAGENET	
	ℓ_∞	ℓ_2	ℓ_∞	ℓ_2	ℓ_∞	ℓ_2
ϵ (allowed perturbation)	0.3	3	12	127	0.05	5
Max allowed queries	10000					
Evaluation/Test set size	1000					
Data (pixel value) Range	[0,1]		[0,255]		[0,1]	

Table 3: Hyperparameters setup for NES

Hyperparameter	Value					
	MNIST		CIFAR10		IMAGENET	
	ℓ_∞	ℓ_2	ℓ_∞	ℓ_2	ℓ_∞	ℓ_2
δ (finite difference probe)	0.1	0.1	2.55	2.55	0.1	0.1
η (image ℓ_p learning rate)	0.1	1	2	127	0.02	2
q (number of finite difference estimations per step)	10	20	20	4	100	50

Table 4: Hyperparameters setup for ZO-SignSGD

Hyperparameter	Value					
	MNIST		CIFAR10		IMAGENET	
	ℓ_∞	ℓ_2	ℓ_∞	ℓ_2	ℓ_∞	ℓ_2
δ (finite difference probe)	0.1	0.1	2.55	2.55	0.1	0.1
η (image ℓ_p learning rate)	0.1	0.1	2	2	0.02	0.004
q (number of finite difference estimations per step)	10	20	20	4	100	50

Table 5: Hyperparameters setup for **Bandits**_{TD}

Hyperparameter	Value					
	MNIST		CIFAR10		IMAGENET	
	ℓ_∞	ℓ_2	ℓ_∞	ℓ_2	ℓ_∞	ℓ_2
η (image ℓ_p learning rate)	0.03	0.01	5	12	0.01	0.1
δ (finite difference probe)	0.1	0.1	2.55	2.55	0.1	0.1
τ (online convex optimization learning rate)	0.001	0.0001	0.0001	1e-05	0.0001	0.1
Tile size (data-dependent prior)	8	10	20	20	50	50
ζ (bandit exploration)	0.01	0.1	0.1	0.1	0.01	0.1

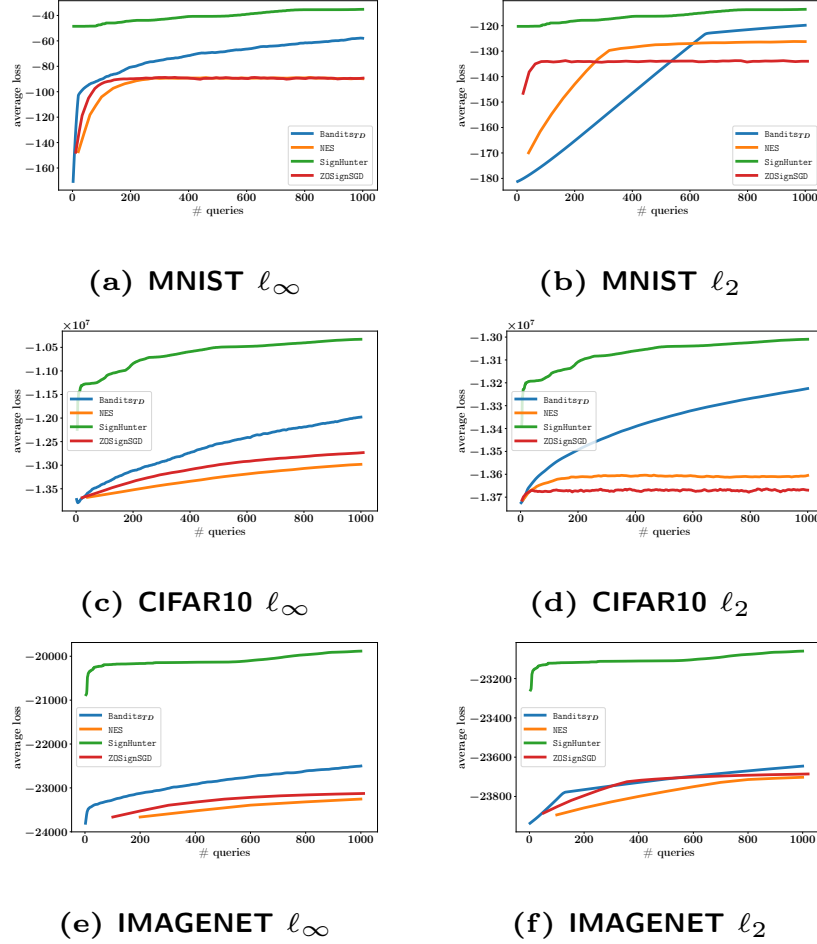


Figure 12: Tuning testbed for the attacks. A synthetic loss function was used to tune the performance of the attacks over a random sample of 25 images for each dataset and ℓ_p perturbation constraint. The plots above show the average performance of the tuned attacks on the synthetic loss function $L(\mathbf{x}, y) = -(\mathbf{x} - \mathbf{x}^*)^T(\mathbf{x} - \mathbf{x}^*)$, where $\mathbf{x}^* = \frac{\mathbf{x}_{min} + \mathbf{x}_{max}}{2}$ using a query limit of 1000 queries for each image. Note that in all, **Bandits_{TD}** outperforms both **NES** and **ZO-SignSGD**. Also, we observe the same behavior reported by [Liu et al. \(2019\)](#) on the fast convergence of **ZO-SignSGD** compared to **NES**. We did not tune **SignHunter**; it does not have any tunable parameters.

Table 6: Hyperparameters setup for **SignHunter**

Hyperparameter	Value					
	MNIST		CIFAR10		IMAGENET	
	ℓ_∞	ℓ_2	ℓ_∞	ℓ_2	ℓ_∞	ℓ_2
δ (finite difference probe)	0.3	3	12	127	0.05	5

Appendix C. Estimating Hamming Oracle

This section illustrates our experiment on the distribution of the magnitudes of gradient coordinates as summarized in Figure 13. *How to read the plots:* Consider the first histogram in Plot (a) from below; it corresponds to the 1000th image from the sampled **MNIST** evaluation set, plotting the histogram of the values $\{|\partial L(\mathbf{x}, y)/\partial x_i|\}_{1 \leq i \leq n}$, where the **MNIST** dataset has dimensionality $n = 784$. These values are in the range $[0, 0.002]$. Overall, the values are fairly concentrated—with exceptions, in Plot (e) for instance, the magnitudes of the $\sim 400^{\text{th}}$ image’s gradient coordinates are spread from 0 to ~ 0.055 . Thus, a Monte Carlo estimate of the mean of $\{|\partial L(\mathbf{x}, y)/\partial x_i|\}_{1 \leq i \leq n}$ would be an appropriate approximation. We release these figures in the form of TensorBoard logs.

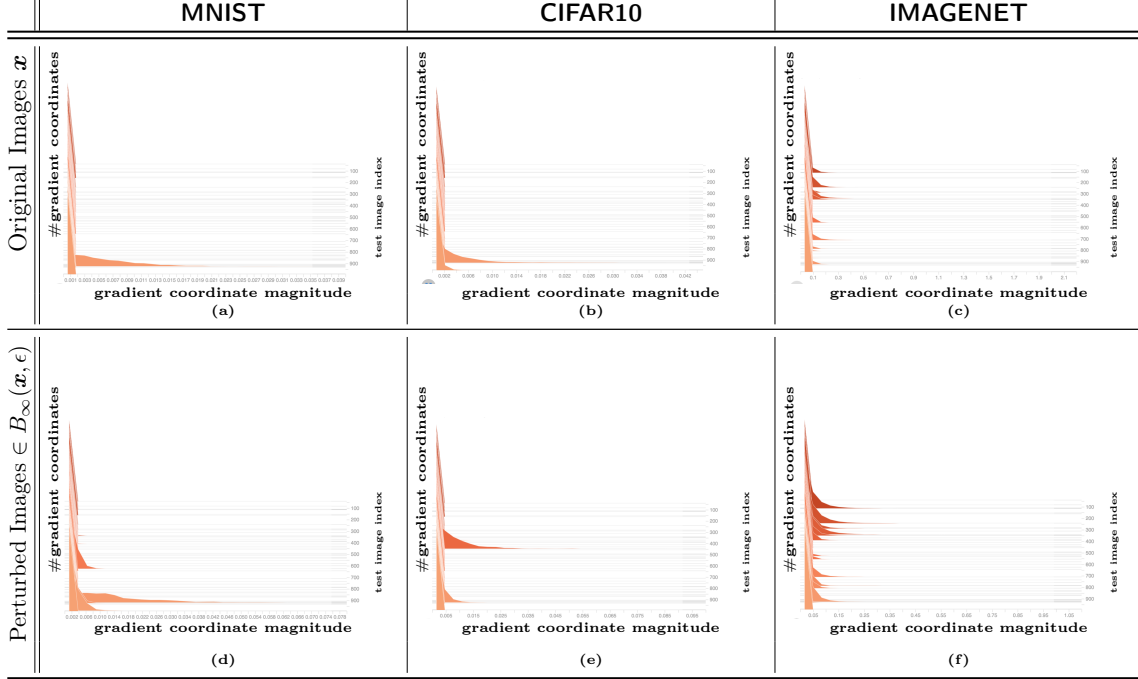


Figure 13: *Magnitudes of gradient coordinates are concentrated:* Plots (a), (b), and (c) show histograms of the magnitudes of gradient coordinates of the loss function $L(\mathbf{x}, y)$ with respect to the input point (image) \mathbf{x} for **MNIST**, **CIFAR10**, and **IMAGENET** neural net models over 1000 images from the corresponding evaluation set, respectively. Plots (d), (e), (f) show the same but at input points (images) sampled randomly within $B_\infty(\mathbf{x}, \epsilon)$: the ℓ_∞ -ball of radius $\epsilon = 0.3, 12$, and 0.05 around the images in Plots (a), (b), and (c), respectively.

Appendix D. Results of Adversarial Black-Box Examples Generation

This section shows results of our experiments in crafting adversarial black-box examples in the form of tables and performance traces, namely Figures 14, 15, and 16; and Tables 7, 8, and 9.

Table 7: Summary of attacks effectiveness on **MNIST** under ℓ_∞ and ℓ_2 perturbation constraints, and with a query limit of 10,000 queries. The *Failure Rate* $\in [0, 1]$ column lists the fraction of failed attacks over 1000 images. The *Avg. # Queries* column reports the average number of queries made to the loss oracle only over successful attacks.

Attack	Failure Rate		Avg. # Queries	
	ℓ_∞	ℓ_2	ℓ_∞	ℓ_2
Bandits _{TD}	0.68	0.59	328.00	673.16
NES	0.63	0.63	235.07	361.42
SignHunter	0.00	0.04	11.06	1064.22
ZOSignSGD	0.63	0.75	157.00	881.08

Table 8: Summary of attacks effectiveness on **CIFAR10** under ℓ_∞ and ℓ_2 perturbation constraints, and with a query limit of 10,000 queries. The *Failure Rate* $\in [0, 1]$ column lists the fraction of failed attacks over 1000 images. The *Avg. # Queries* column reports the average number of queries made to the loss oracle only over successful attacks.

Attack	Failure Rate		Avg. # Queries	
	ℓ_∞	ℓ_2	ℓ_∞	ℓ_2
Bandits _{TD}	0.95	0.39	432.24	1201.85
NES	0.37	0.67	312.57	496.99
SignHunter	0.07	0.21	121.00	692.39
ZOSignSGD	0.37	0.80	161.28	528.35

Table 9: Summary of attacks effectiveness on **IMAGENET** under ℓ_∞ and ℓ_2 perturbation constraints, and with a query limit of 10,000 queries. The *Failure Rate* $\in [0, 1]$ column lists the fraction of failed attacks over 1000 images. The *Avg. # Queries* column reports the average number of queries made to the loss oracle only over successful attacks.

Attack	Failure Rate		Avg. # Queries	
	ℓ_∞	ℓ_2	ℓ_∞	ℓ_2
Bandits _{TD}	0.07	0.11	1010.05	1635.55
NES	0.26	0.42	1536.19	1393.86
SignHunter	0.02	0.23	578.56	1985.55
ZOSignSGD	0.23	0.52	1054.98	931.15

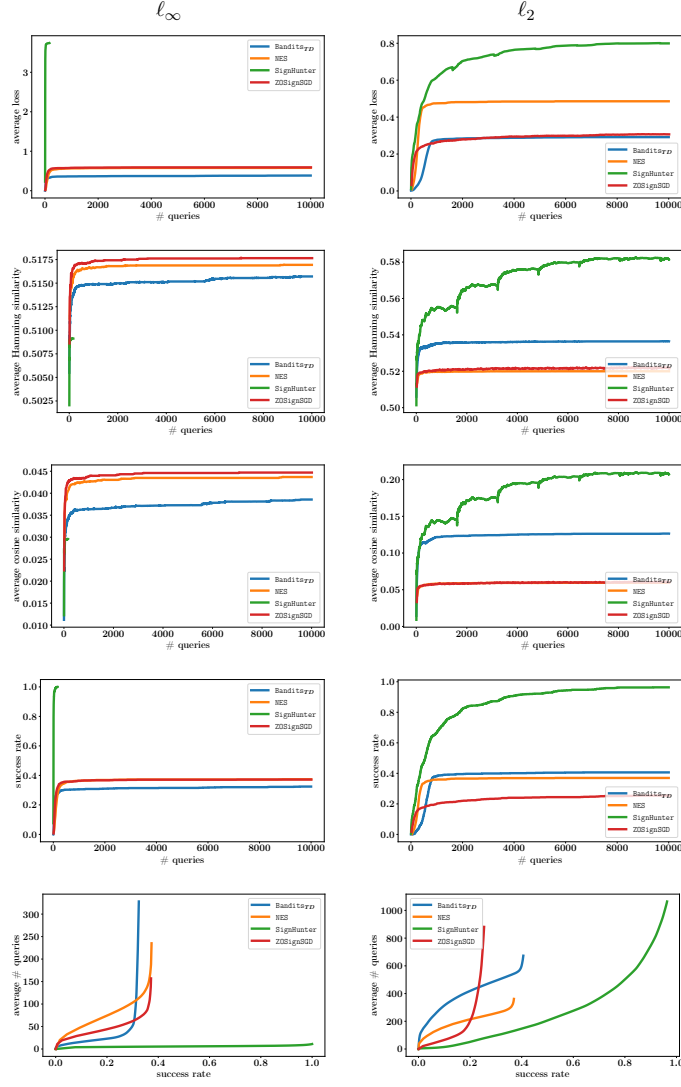


Figure 14: Performance curves of attacks on **MNIST** for ℓ_∞ (first column) and ℓ_2 (second column) perturbation constraints. Plots of *Avg. Loss* row reports the loss as a function of the number of queries averaged over all images. The *Avg. Hamming Similarity* row shows the Hamming similarity of the sign of the attack’s estimated gradient $\hat{\mathbf{g}}$ with true gradient’s sign \mathbf{q}^* , computed as $1 - \|\text{sign}(\hat{\mathbf{g}}) - \mathbf{q}^*\|_H/n$ and averaged over all images. Likewise, plots of the *Avg. Cosine Similarity* row show the normalized dot product of $\hat{\mathbf{g}}$ and \mathbf{g}^* averaged over all images. The *Success Rate* row reports the attacks’ cumulative distribution functions for the number of queries required to carry out a successful attack up to the query limit of 10,000 queries. The *Avg. # Queries* row reports the average number of queries used per successful image for each attack when reaching a specified success rate: the more effective the attack, the closer its curve is to the bottom right of the plot.

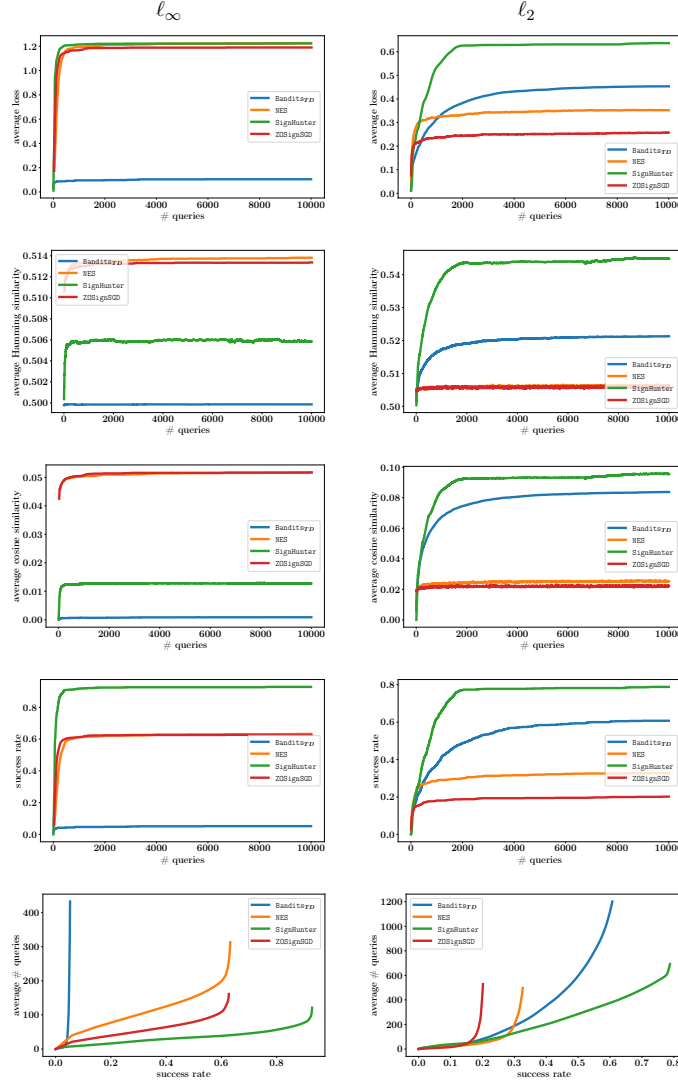


Figure 15: Performance curves of attacks on **CIFAR10** for ℓ_∞ (first column) and ℓ_2 (second column) perturbation constraints. Plots of *Avg. Loss* row reports the loss as a function of the number of queries averaged over all images. The *Avg. Hamming Similarity* row shows the Hamming similarity of the sign of the attack’s estimated gradient $\hat{\mathbf{g}}$ with true gradient’s sign \mathbf{q}^* , computed as $1 - \|\text{sign}(\hat{\mathbf{g}}) - \mathbf{q}^*\|_H/n$ and averaged over all images. Likewise, plots of the *Avg. Cosine Similarity* row show the normalized dot product of $\hat{\mathbf{g}}$ and \mathbf{g}^* averaged over all images. The *Success Rate* row reports the attacks’ cumulative distribution functions for the number of queries required to carry out a successful attack up to the query limit of 10,000 queries. The *Avg. # Queries* row reports the average number of queries used per successful image for each attack when reaching a specified success rate: the more effective the attack, the closer its curve is to the bottom right of the plot.

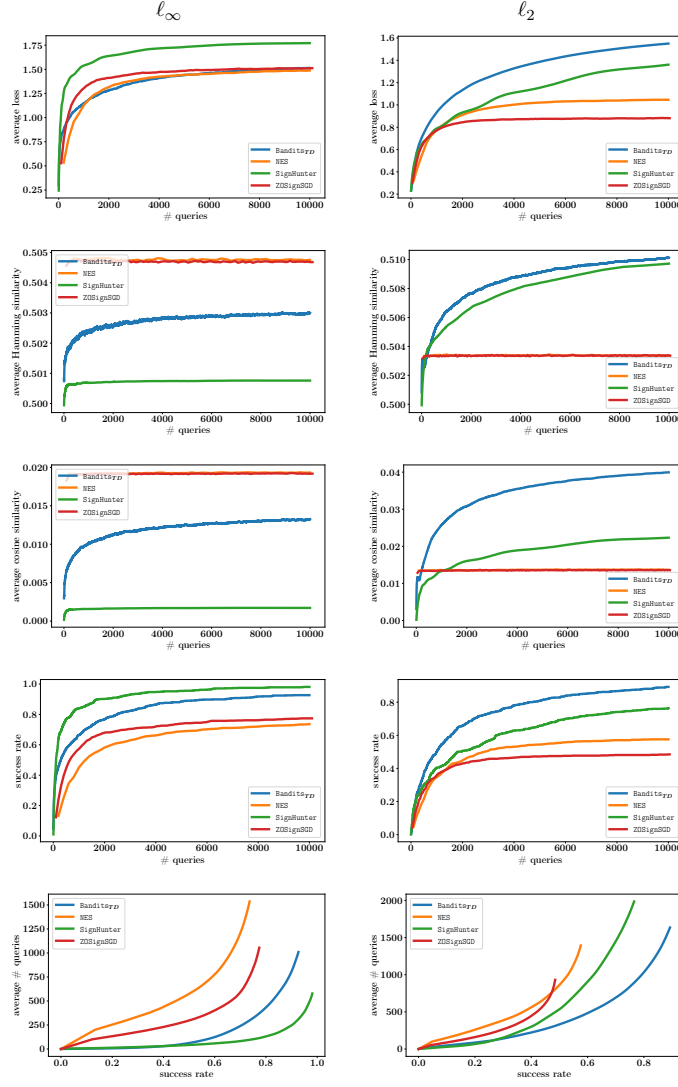


Figure 16: Performance curves of attacks on **IMAGENET** for ℓ_∞ (first column) and ℓ_2 (second column) perturbation constraints. Plots of *Avg. Loss* row reports the loss as a function of the number of queries averaged over all images. The *Avg. Hamming Similarity* row shows the Hamming similarity of the sign of the attack’s estimated gradient $\hat{\mathbf{g}}$ with true gradient’s sign \mathbf{q}^* , computed as $1 - \|\text{sign}(\hat{\mathbf{g}}) - \mathbf{q}^*\|_H/n$ and averaged over all images. Likewise, plots of the *Avg. Cosine Similarity* row show the normalized dot product of $\hat{\mathbf{g}}$ and \mathbf{g}^* averaged over all images. The *Success Rate* row reports the attacks’ cumulative distribution functions for the number of queries required to carry out a successful attack up to the query limit of 10,000 queries. The *Avg. # Queries* row reports the average number of queries used per successful image for each attack when reaching a specified success rate: the more effective the attack, the closer its curve is to the bottom right of the plot.